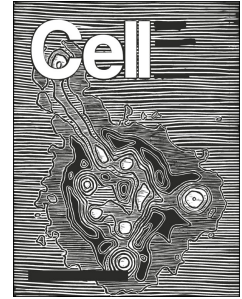


Journal Pre-proof



Circular RNA Vaccines against SARS-CoV-2 and Emerging Variants

Liang Qu, Zongyi Yi, Yong Shen, Liangru Lin, Feng Chen, Yiyuan Xu, Zeguang Wu, Huixian Tang, Xiaoxue Zhang, Feng Tian, Chunhui Wang, Xia Xiao, Xiaojing Dong, Li Guo, Shuaiyao Lu, Chengyun Yang, Cong Tang, Yun Yang, Wenhai Yu, Junbin Wang, Yanan Zhou, Qing Huang, Ayijiang Yisimayi, Shuo Liu, Weijin Huang, Yunlong Cao, Youchun Wang, Zhuo Zhou, Xiaozhong Peng, Jianwei Wang, Xiaoliang Sunney Xie, Wensheng Wei

PII: S0092-8674(22)00394-4

DOI: <https://doi.org/10.1016/j.cell.2022.03.044>

Reference: CELL 12432

To appear in: *Cell*

Received Date: 12 January 2022

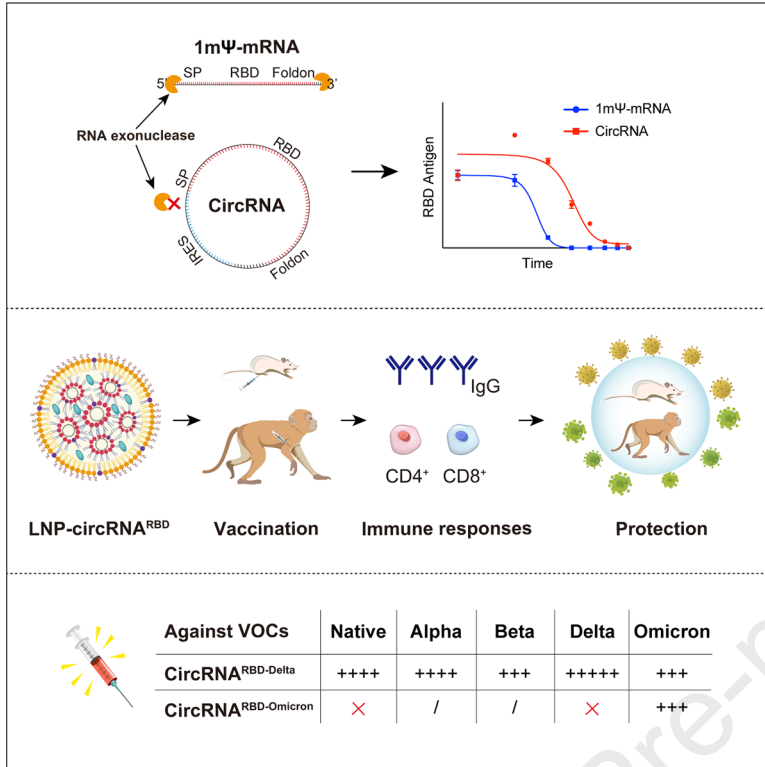
Revised Date: 11 March 2022

Accepted Date: 30 March 2022

Please cite this article as: Qu, L., Yi, Z., Shen, Y., Lin, L., Chen, F., Xu, Y., Wu, Z., Tang, H., Zhang, X., Tian, F., Wang, C., Xiao, X., Dong, X., Guo, L., Lu, S., Yang, C., Tang, C., Yang, Y., Yu, W., Wang, J., Zhou, Y., Huang, Q., Yisimayi, A., Liu, S., Huang, W., Cao, Y., Wang, Y., Zhou, Z., Peng, X., Wang, J., Xie, X.S., Wei, W., Circular RNA Vaccines against SARS-CoV-2 and Emerging Variants, *Cell* (2022), doi: <https://doi.org/10.1016/j.cell.2022.03.044>.

This is a PDF file of an article that has undergone enhancements after acceptance, such as the addition of a cover page and metadata, and formatting for readability, but it is not yet the definitive version of record. This version will undergo additional copyediting, typesetting and review before it is published in its final form, but we are providing this version to give early visibility of the article. Please note that, during the production process, errors may be discovered which could affect the content, and all legal disclaimers that apply to the journal pertain.

© 2022 The Author(s). Published by Elsevier Inc.



Circular RNA Vaccines against SARS-CoV-2 and Emerging Variants

Liang Qu,^{1,8} Zongyi Yi,^{1,2,8} Yong Shen,^{1,2,8} Liangru Lin,¹ Feng Chen,^{1,2} Yiyuan Xu,¹ Zeguang Wu,¹ Huixian Tang,¹ Xiaoxue Zhang,^{1,2} Feng Tian,¹ Chunhui Wang,¹ Xia Xiao,³ Xiaojing Dong,³ Li Guo,³ Shuaiyao Lu,⁴ Chengyun Yang,⁴ Cong Tang,⁴ Yun Yang,⁴ Wenhai Yu,⁴ Junbin Wang,⁴ Yanan Zhou,⁴ Qing Huang,⁴ Ayijiang Yisimayi,⁵ Shuo Liu,⁶ Weijin Huang,⁶ Yunlong Cao,⁵ Youchun Wang,⁶ Zhuo Zhou,¹ Xiaozhong Peng,^{4,7} Jianwei Wang,³ Xiaoliang Sunney Xie,⁵ Wensheng Wei^{1,9,*}

¹Biomedical Pioneering Innovation Center, Beijing Advanced Innovation Center for Genomics, Peking-Tsinghua Center for Life Sciences, Peking University Genome Editing Research Center, State Key Laboratory of Protein and Plant Gene Research, School of Life Sciences, Peking University, Beijing 100871, P.R. China.

²Academy for Advanced Interdisciplinary Studies, Peking University, Beijing 100871, China.

³NHC Key Laboratory of Systems Biology of Pathogens and Christophe Mérieux Laboratory, Institute of Pathogen Biology, Chinese Academy of Medical Sciences and Peking Union Medical College, Beijing 100730, China; Key Laboratory of Respiratory Disease Pathogenomics, Chinese Academy of Medical Sciences and Peking Union Medical College, Beijing 100730, China.

⁴National Kunming High-level Biosafety Primate Research Center, Institute of Medical Biology, Chinese Academy of Medical Sciences and Peking Union Medical College, Yunnan China.

⁵Biomedical Pioneering Innovation Center, Beijing Advanced Innovation Center for Genomics, Peking-Tsinghua Center for Life Sciences, Peking University, Beijing 100871, China.

⁶Division of HIV/AIDS and Sex-transmitted Virus Vaccines, Institute for Biological Product Control, National Institutes for Food and Drug Control (NIFDC) and WHO Collaborating Center for Standardization and Evaluation of Biologicals, Beijing 102629, China.

⁷State Key Laboratory of Medical Molecular Biology, Department of Molecular Biology and Biochemistry, Institute of Basic Medical Sciences, Medical Primate Research Center, Neuroscience Center, Chinese Academy of Medical Sciences, School of Basic Medicine Peking Union Medical College, Beijing 100730, China.

30

31 ⁸These authors contributed equally32 ⁹Lead contact

33 *Correspondence: wswei@pku.edu.cn (W.W.)

34

35 **SUMMARY**

36 As the emerging variants of SARS-CoV-2 continue to drive the worldwide pandemic, there is a
37 constant demand for vaccines that offer more effective and broad-spectrum protection. Here, we
38 report a circular RNA (circRNA) vaccine that elicited potent neutralizing antibodies and T cell
39 responses by expressing the trimeric RBD of the spike protein, providing robust protection against
40 SARS-CoV-2 in both mice and rhesus macaques. Notably, the circRNA vaccine enabled higher
41 and more durable antigen production than the 1m Ψ -modified mRNA vaccine, and elicited a higher
42 proportion of neutralizing antibodies and distinct Th1-skewed immune responses. Importantly, we
43 found that the circRNA^{RBD-Omicron} vaccine induced effective neutralizing antibodies against the
44 Omicron but not the Delta variant. In contrast, the circRNA^{RBD-Delta} vaccine protected against both
45 Delta and Omicron or functioned as a booster after two doses of either native- or Delta-specific
46 vaccination, making it a favorable choice against the current variants of concern (VOCs) of SARS-
47 CoV-2.

48

49

50 **INTRODUCTION**

51 Coronavirus disease 2019 (COVID-19) is a serious worldwide public health emergency caused by
52 a severe acute respiratory syndrome coronavirus (SARS-CoV-2) (Wu et al., 2020; Zhou et al.,
53 2020). To date, COVID-19 has resulted in over 470 million confirmed cases and over 6 million
54 confirmed deaths (World Health Organization). With the development of the epidemic, variants
55 with immune escape ability have appeared, the most serious of which is Omicron. By the end of
56 January, 2022, Omicron accounted for ~85% of COVID-19 cases (GISAID). Omicron carries over
57 30 mutations on the spike protein, 15 of which are located in the receptor-binding domain (RBD)
58 (Dejnirattisai et al., 2022), resulting in a significant decrease in the effectiveness of prior

59 neutralizing antibodies (Cameroni et al., 2021; Cao et al., 2021; Cele et al., 2021; Liu et al., 2021c;
60 Planas et al., 2021a). Although it has recently been reported that an additional boost with original
61 SARS-CoV-2 vaccines after receiving two-dose prior vaccination could partly elevate the
62 neutralizing capability, the neutralization of Omicron pseudovirus was 4~13-fold lower than that
63 of the wild type (Garcia-Beltran et al., 2022). This poses a severe challenge to the efficacy of
64 current vaccines, highlighting the urgent need to develop effective vaccines against such fast-
65 spreading variants.

66 SARS-CoV-2 belongs to the genus *Betacoronavirus* of the *Coronaviridae* family (V'Kovski et
67 al., 2021). SARS-CoV-2 is a single-strand, positive-sense, enveloped virus, with an inner capsid
68 formed by a 30-kb RNA genome wrapped by the nucleocapsid (N) proteins and a lipid envelope
69 coated with the membrane (M), envelope (E), and spike (S) proteins (Kim et al., 2020). The S
70 protein of SARS-CoV-2, composed of the S1 and S2 subunits, is the major surface protein of the
71 virion. The S protein mediates viral entry into host cells by binding to its receptor, angiotensin-
72 converting enzyme 2 (ACE2), through the receptor-binding domain (RBD) at the C-terminus of
73 the S1 subunit. This binding subsequently induces the fusion between the SARS-CoV-2 envelope
74 and the host cell membrane mediated by the S2 subunit, which leads to the release of the viral
75 genome into the cytoplasm (Hoffmann et al., 2020; Shang et al., 2020; Wrapp et al., 2020; Yan et
76 al., 2020).

77 The S protein, S1 subunit, or RBD antigen of SARS-CoV-2 can induce both B cell and T cell
78 responses, generating highly potent neutralizing antibodies against SARS-CoV-2 (Bangaru et al.,
79 2020; Hsieh et al., 2020; Walls et al., 2020). Vaccination is the most promising approach to end
80 the COVID-19 pandemic. Traditional vaccine platforms, such as inactivated, virus-like particle,
81 and viral vector-based vaccines have been adopted to develop SARS-CoV-2 vaccines (Dai et al.,
82 2020; Gao et al., 2020; Krammer, 2020; Mullard, 2020; Sanchez-Felipe et al., 2021; van
83 Doremalen et al., 2020; Yang et al., 2020; Yu et al., 2020; Zhu et al., 2020). Importantly, mRNA
84 vaccines against SARS-CoV-2 have been developed at warp speed and rapidly approved for use
85 (Corbett et al., 2020a; Corbett et al., 2020b; Huang et al., 2021; Laczko et al., 2020; Sahin et al.,
86 2020; Vogel et al., 2021; Zhang et al., 2020), even though the strategy was still in clinical trials
87 and had never been applied commercially before (Pardi et al., 2018). The mRNA vaccine contains
88 a linear single-stranded RNA consisting of a 5' cap, the untranslated region (UTR), the antigen-
89 coding region, and a 3' polyA tail and is delivered into the body via lipid-nano particle (LNP)

90 encapsulation (Pardi et al., 2018). The clinical-scale mRNA vaccines could be manufactured
91 rapidly upon the release of the viral antigen sequence (Corbett et al., 2020a). However, due to its
92 susceptibility to exonuclease digestion, the current mRNA vaccine still has certain limitations
93 including inherent instability and suboptimal thermostability after LNP encapsulation for *in vivo*
94 administration (Durymanov and Reineke, 2018; Fenton et al., 2016; Jackson et al., 2020).
95 Therefore, mRNA vaccine manufacturing necessitates extremely sterile and strictly RNase-free
96 environment during the whole production process, and its storage and distribution often requires
97 low temperature cold-chain, limiting its availability in lower-resource countries or regions (Uddin
98 and Roni, 2021). Furthermore, because the mRNA produced by *in vitro* transcription (IVT) has a
99 rather short half-life in cells, it requires additional nucleotide modifications (e.g. 1-
100 methylpseudouridine) to improve its stability while reducing the risk of unwanted immunogenicity
101 (Kariko et al., 2005; Pardi et al., 2018).

102 Unlike the linear conformation of mRNA, circular RNAs (circRNAs) are covalently closed ring
103 RNA molecules that comprise a large class of noncoding RNAs generated in eukaryotic cells by a
104 noncanonical RNA splicing event called backsplicing in eukaryotic cells (Chen, 2016; Kristensen
105 et al., 2019; Zhang et al., 2014). Compared to the linear mRNA, circRNA is highly stable due to
106 its covalently closed ring structure, which protects it from exonuclease-mediated degradation
107 (Enuka et al., 2016; Kristensen et al., 2019; Memczak et al., 2013). It has been reported that
108 circRNAs were more stable than their linear mRNA counterparts, with the circRNAs having the
109 median half-life at least 2.5 times longer than their linear mRNA isoforms in mammalian cells
110 (Enuka et al., 2016; Kristensen et al., 2019; Memczak et al., 2013). To date, only a few endogenous
111 circRNAs have been shown to function as protein translation templates (Gao et al., 2021; Legnini
112 et al., 2017; Zhang et al., 2018a; Zhang et al., 2018b). Although circRNA lacks the essential
113 elements for cap-dependent translation, it can be engineered to enable protein translation through
114 an internal ribosome entry site (IRES) or the incorporation of the m6A modification upstream of
115 the open reading frame (ORF) (Wesselhoeft et al., 2018; Yang et al., 2017). Thus, we envisioned
116 that circRNA could be leveraged as a platform to generate immunogens.

117 Although the potential immunogenicity of IVT-produced circRNA has been a source of debates
118 (Chen et al., 2019; Liu et al., 2021b; Wesselhoeft et al., 2019), it is tempting to test whether
119 circRNA could be developed into a safe and effective vaccine platform. Given the inherent stability

120 and an avoidable need for nucleotide modifications, we attempted to develop circular RNA
121 vaccines, aiming to provide effective protection against SARS-CoV-2 and its emerging variants.

122

123 **RESULTS**

124 **circRNA^{RBD} produced functional SARS-CoV-2 RBD antigens**

125 We employed the group I intron autocatalysis strategy (Wesselhoeft et al., 2018) to produce
126 circular RNAs encoding SARS-CoV-2 RBD antigens, termed circRNA^{RBD} (Figure 1A). In this
127 construct, the IRES element was placed before the RBD-coding sequence to initiate its translation.
128 To enhance the immunogenicity of RBD antigens, the signal peptide sequence of human tissue
129 plasminogen activator (tPA) was fused to the N-terminus of RBD to ensure the secretion of
130 antigens (Kou et al., 2017; Pardi et al., 2017; Richner et al., 2017). In addition, recent research
131 reported that spike trimers outperformed monomeric spikes in binding hACE2 (Bouwman et al.,
132 2021; Wrapp et al., 2020; Yan et al., 2020). To improve the immunogenicity of RBD antigens, the
133 trimerization motif of bacteriophage T4 fibritin protein (Foldon) (Papanikolopoulou et al., 2008)
134 was fused to its C-terminus. This IRES-SP-RBD-Foldon sequence was then cloned into the vector
135 to construct the IVT template for producing circRNA^{RBD} (Figure 1A; Table S1).

136 To produce high-purity circRNA^{RBD}, we first optimized the IVT reaction to generate
137 circRNA^{RBD} (Figure S1A) without extra step of GTP catalysis (Wesselhoeft et al., 2018). High-
138 performance liquid chromatography (HPLC) analysis determined that the latter half of main peak
139 contained high-purity circRNA (Figures S1B and S1C). Then we successfully manufactured
140 circRNA^{RBD} in large quantities (Figures S1D and S1E). We found that the majority of the purified
141 circRNA^{RBD} fractions were resistant to exonuclease-RNase R, while the nicked RNA^{RBD} were
142 almost completely degraded, indicating that purified circRNA^{RBD} were mostly in circular format
143 (Figure S1F). The purity of circRNA^{RBD} was over 90% calculated via the denaturing gel
144 electrophoresis and the following semi-quantitative analysis (Figures S1G-S1I). The
145 circularization of circRNA^{RBD} was further verified by reverse transcription-PCR, Sanger
146 sequencing and RNase H-mediated specific cleavage (Figures S1J-S1M).

147 To test the secretory expression of RBD produced by circRNA^{RBD}, the purified circRNA^{RBD}
148 was transfected into HEK293T cells or NIH3T3 cells. Abundant RBD antigens in the supernatant
149 of both human and murine cells were detected by Western blot, indicating the high compatibility

150 of circRNAs (Figure 1B). With the help of Foldon, the circRNA^{RBD} encoded stable homogeneous
151 RBD trimers in the supernatant, which were dissociated into monomers under reducing conditions
152 (Figure 1C). The concentration of RBD antigens produced by circRNA^{RBD} reached ~1,400 ng/ml,
153 600-fold higher than those produced by its linear precursor RNA (Figure 1D).

154 In addition to the group I intron-based strategy, we also developed a T4 RNA ligase-based
155 method to produce circular RNAs. This method adopted the complementary pairing sequence of
156 split IRES as the splint instead of a DNA splint to generate an intramolecular RNA nick structure
157 serving as the catalytic substrate of T4 RNA ligase (Figure S2A; Table S2). Sanger sequencing
158 confirmed the precise circularization of circRNA^{RBD} by this approach (Figure S2B). Similarly,
159 abundant RBD antigens were detected in the supernatant at a concentration of ~1,000 ng/ml, which
160 was ~200-fold higher than those produced by its linear precursor RNA (Figures S2C and S2D).

161 To verify whether the secreted SARS-CoV-2 RBD antigens produced by circRNA^{RBD} were
162 functional, the supernatants of circRNA^{RBD}-transfected cells were used in a competition assay
163 using hACE2-overexpressing HEK293 cells (HEK293T-ACE2) and SARS-CoV-2 pseudovirus
164 harboring an EGFP reporter (Ou et al., 2020). The secreted RBD antigens could effectively block
165 SARS-CoV-2 pseudovirus infection (Figure 1E).

166

167 **SARS-CoV-2 circRNA^{RBD} vaccine induced sustained humoral immune responses with high** 168 **levels of neutralizing antibodies**

169 To explore whether circRNA could be leveraged to create a vaccine, we attempted to assess the
170 immunogenicity of circRNA^{RBD} encapsulated with LNP in BALB/c mice (Figure 1F). The
171 circRNA^{RBD} encapsulation efficiency was greater than 93%, with an average diameter of 100 nm
172 (Figure 1G). Mice were immunized through intramuscular (i.m.) injection with 10 µg or 50 µg of
173 LNP-circRNA^{RBD} vaccines twice at a two-week interval (Figure 1H). The circRNA^{RBD} elicited a
174 high level of RBD-specific IgG endpoint geometric mean titers (GMTs), reaching $\sim 1.9 \times 10^4$ for
175 the 10 µg dose and $\sim 5.7 \times 10^5$ for the 50 µg dose (Figure 1I).

176 Sera from circRNA^{RBD}-vaccinated mice effectively neutralized SARS-CoV-2 pseudovirus
177 with a 50% neutralization titer (NT50) of $\sim 4.5 \times 10^3$ (Figure 1J) and authentic SARS-CoV-2 virus
178 with an NT50 of $\sim 7.0 \times 10^4$ (Figure 1K).

179

180 **SARS-CoV-2 circRNA^{RBD-Beta} vaccine-elicited antibodies showed preferential neutralizing**
181 **activity against the Beta variant**

182 Next, we evaluated the efficacy of circRNA^{RBD-Beta}, a circRNA vaccine encoding RBD/K417N-
183 E484K-N501Y antigens derived from the SARS-CoV-2 Beta variant. Mice were immunized with
184 LNP-circRNA^{RBD-Beta} through i.m. injection twice at a two-week interval. The immunized mice's
185 sera were collected at 1 and 2 weeks after the boost. ELISA showed that the RBD-Beta-specific
186 IgG endpoint GMT was $\sim 1.6 \times 10^4$ at one week after the boost (Figure 1L). Pseudovirus
187 neutralization assays revealed that circRNA^{RBD}-elicited antibodies could effectively neutralize all
188 three pseudoviruses, with the highest neutralizing activity against the native (D614G) strain
189 (Figure 1M). The circRNA^{RBD-Beta}-elicited antibodies could also neutralize all three pseudoviruses,
190 with the highest activity against its corresponding Beta variant (Figure 1N).

191 In line with pseudovirus neutralization assay, the sera from immunized mice neutralized the
192 authentic SARS-CoV-2 Beta and native (D614G) strains with NT50 values of 2.6×10^4 (Figure 1O)
193 and 6.0×10^3 (Figure 1P), respectively.

194

195 **CircRNA^{RBD-Beta} vaccine protected mice against infection with the Beta variant**

196 To further evaluate the protective efficacy of circRNA^{RBD-Beta} vaccine, we employed the authentic
197 Beta variant for challenge experiments. Consistent with a recent report (Chen et al., 2021;
198 Montagutelli et al., 2021), the Beta variant could infect wild-type BALB/c mice and replicate in
199 their lungs (Figure 1Q), likely due to mutations in the spike such as K417N, E484K, and N501Y.
200 Seven weeks after the boost dose, the RBD-Beta-specific IgG endpoint GMT was still
201 approximately 1.2×10^4 (Figure 1R), with significant neutralizing activity against RBD-Beta
202 antigens (Figure 1S). Each immunized mouse was then intranasally infected with 5×10^4 PFU
203 (plaque forming unit) of Beta virus (7 weeks post boost). Lung tissues were collected three days
204 after the challenge for the detection of viral RNAs. The viral loads in the lungs of circRNA-
205 vaccinated mice were significantly lower than those of the placebo group (Figure 1T). Consistently,
206 only the mice in the placebo group exhibited weight loss (Figure 1U). These results indicated that
207 the circRNA^{RBD-Beta} vaccine could effectively protect the mice against SARS-CoV-2 Beta.

208 Considering that high dose of circRNA^{RBD} was necessary to elicit maximal level of neutralizing
209 antibodies, we postulated that the LNP delivery platform might have a great impact on the efficacy
210 of the circular RNA vaccine. After multiple tests, we were able to significantly lower the vaccine
211 dose using one of the commercial formulas (Precision Nanosystems). Ten micrograms of circRNA
212 could induce neutralizing antibodies at a comparable level to 50 µg (Figure 1V). We thus switched
213 our choice of LNP for the rest of our experiments.

214

215 **CircRNA^{RBD-Delta} vaccine induced potent neutralizing antibodies against SARS-CoV-2 Delta**

216 The Delta variant, like the Beta variant, partially escapes the antibodies produced in survivors or
217 vaccinees (Lustig et al., 2021; Planas et al., 2021b; Torgovnick, 2021). To develop such a variant-
218 specific vaccine, we adopted both group I intron and T4 RNA ligase ligation strategies to produce
219 circRNA^{RBD-Delta}. Mice were immunized i.m. with 0.5 µg, 2.5 µg, 5 µg or 10 µg of circRNA<sup>RBD-
220 Delta</sup> vaccines twice at a two-week interval. Two weeks after the boost dose, the sera from
221 immunized mice were collected to detect RBD-Delta-specific antibodies. Vaccines of circRNA<sup>RBD-
222 Delta</sup> made by either circularization method could induce high endpoint GMTs (Figures 2A and 2B).
223 The sera from circRNA^{RBD-Delta}-vaccinated mice effectively neutralized the Delta pseudovirus in a
224 dose-dependent manner, with an NT50 of $\sim 1.4 \times 10^5$ for the 10 µg dose (Figure 2C).

225 Importantly, circRNA^{RBD-Delta} vaccines could provide protection against other variants,
226 including the native strain, Alpha and Beta, albeit to varying degrees. The sera from circRNA<sup>RBD-
227 Delta</sup>-immunized mice exhibited the highest neutralizing activity against Delta and the lowest
228 against Beta (Figures 2D and 2E).

229

230 **CircRNA vaccine enabled higher and more durable antigen expression than mRNA vaccine**

231 CircRNAs are reportedly more stable than mRNAs owing to their covalent closed circular structure
232 (Fischer and Leung, 2017). To test whether the stability of the circRNA vaccine could confer higher
233 and more durable antigen-encoding efficiency than the mRNA vaccine, we generated 1mΨ-
234 modified mRNA (1mΨ-mRNA), and unmodified mRNA, both of which contained the same RBD-
235 encoding sequence as the circRNA for a fair comparison (Figure S3A; Table S3). The circRNA
236 produced much higher levels of RBD antigens at all time points than both 1mΨ-mRNA and

237 unmodified mRNA, and they were maintained for a longer period (Figure 3A). RT-qPCR showed
238 that circRNAs were more stable than mRNAs, modified or unmodified (Figure 3B). Importantly,
239 LNP encapsulation further enhanced the advantage of circRNA in protein production and
240 durability from both 1m Ψ -mRNA and unmodified-mRNA (Figure 3C). Interestingly, LNP
241 encapsulation appeared to improve the antigen-encoding efficiency of unmodified mRNA to a
242 level comparable to that of 1m Ψ -mRNA (Figure 3C).

243 We found that even after two weeks of storage at room temperature ($\sim 25^{\circ}\text{C}$), the circRNA could
244 express RBD antigens without detectable loss (Figure 3D), highlighting its remarkable thermal
245 stability. To further evaluate the thermostability of the vaccines, the LNP-encapsulated circRNA,
246 1m Ψ -mRNA and unmodified mRNA were stored at 4°C , $\sim 25^{\circ}\text{C}$, or 37°C for up to 28 days prior
247 to transfection. At all temperatures tested, circRNA expressed higher levels of antigens than those
248 of the other two mRNA groups (Figures S3B-S3D). At 4°C , little reduction in RBD antigens
249 produced by LNP-circRNA could be detected from 1-28 days (Figure S3B). The stability of LNP-
250 circRNA, 1m Ψ -mRNA or unmodified-mRNA was clearly reduced with increasing storage
251 temperature, especially at 37°C (Figures S3C and S3D).

252 Importantly, we found that the innate immune responses elicited by LNP-encapsulated RNAs
253 were comparable to those by LNP-encapsulated 1m Ψ -mRNA^{RBD}, and significantly lower than
254 those by the transfected RNAs (Figure 3E).

255

256 **CircRNA vaccine elicited higher surrogate IgG ratios of Th1-biased responses and elevated** 257 **proportions of neutralizing antibodies than mRNA vaccine**

258 Given that circRNA vaccines possess higher stability and antigen-encoding efficiency, we
259 wondered whether they exhibited distinctive immunogenicity compared to mRNA vaccines. We
260 compared the balance of Th1/Th2 immune responses between circRNA^{RBD-Delta} and mRNA^{RBD-Delta}
261 vaccines because Th2-biased immune responses might induce vaccine-associated enhanced
262 respiratory disease (VAERD) (Corbett et al., 2020a; Graham, 2020; Sahin et al., 2020). ELISA
263 showed that the total IgG elicited by circRNA^{RBD-Delta} was comparable to that by 1m Ψ -mRNA^{RBD-}
264 ^{Delta} (Figure 3F), however, the ratios of IgG2a/IgG1, IgG2c/IgG1 or (IgG2a + IgG2c)/IgG1 from
265 circRNA^{RBD-Delta} were consistently higher than those from 1m Ψ -mRNA^{RBD-Delta} vaccine (Figures
266 3G, 3H, S3E and S3F), and this Th1-skewed T cell immune response was believed beneficial for

267 the clearance of SARS-CoV-2 (Corbett et al., 2020a; Graham, 2020; Sahin et al., 2020).

268 Antibody-dependent enhancement (ADE) of infection by virus-specific antibodies is another
269 potential concern for vaccines that has been reported for infections by some viruses, including
270 Zika, Dengue, and coronaviruses (Dowd and Pierson, 2011; Halstead and O'Rourke, 1977; Rey et
271 al., 2018; Takano et al., 2019; Wen et al., 2020). Previous research has reported that virus-binding
272 antibodies without neutralizing activity elicited by infection or vaccination possibly caused ADE
273 effects, especially for those viruses with different serotypes (Dejnirattisai et al., 2010; Martinez-
274 Vega et al., 2017). Therefore, we compared the ratios of neutralizing to binding antibodies between
275 circRNA and 1m Ψ -mRNA vaccines. Although circRNA^{RBD-Delta} exhibited equal neutralizing
276 capability to 1m Ψ -mRNA^{RBD-Delta} (Figures 3I-3L), the former induced higher proportions of
277 neutralizing antibodies at both 2.5 μ g and 10 μ g doses in mice (Figure 3M). Owing to this unique
278 feature, the circRNA vaccine might have a certain advantage in circumventing potential ADE
279 effects caused by viruses such as Dengue and Zika and better tolerating frequent viral mutations.

280

281 **CircRNA^{RBD-Delta} vaccine elicited SARS-CoV-2 specific T cell immune responses**

282 B cells, CD4⁺ T cells, and CD8⁺ T cells mediated effector functions against SARS-CoV-2 in
283 COVID-19 patients (Sette and Crotty, 2021). To compare CD4⁺ and CD8⁺ T cell immune
284 responses, the splenocytes of immunized mice were collected and stimulated with SARS-CoV-2
285 RBD-Delta pooled peptides (Table S4), and cytokine-producing T cells were quantified by
286 intracellular cytokine staining among effector memory T cells (Tem, CD44⁺CD62L⁻) (Figure S4).
287 After stimulation with peptides, CD8⁺ T cells producing IFN- γ , TNF- α , and IL-2 were detected in
288 mice immunized with the circRNA^{RBD-Delta} vaccine or 1m Ψ -mRNA^{RBD-Delta} vaccine (Figures 4A-
289 4C), indicating the RBD-specific CD8⁺ T cell responses elicited by both vaccines. The CD4⁺ T
290 cells of immunized mice induced strong IFN- γ , TNF- α , and IL-2 responses but minimal IL-4
291 responses (Figures 4D-4G). In consistent to the above results (Figures 3G, 3H, S3E and S3F), these
292 indicated that circRNA vaccines induced Th1-biased T cell immune responses (Figures 4D-4G
293 and S5A-S5D).

294

295 **CircRNA^{RBD-Delta} vaccine elicited high levels of broad-spectrum neutralizing antibodies**
296 **against both the Delta and Omicron variants**

297 To cope with the current Omicron emergency, we tested the neutralizing capability elicited by all
298 three circRNA vaccines against the Omicron variant. The neutralizing activity against Omicron
299 elicited by either one of the three circRNA vaccines dropped 74-fold (native), 15-fold (Beta) and
300 44-fold (Delta) in comparison with the neutralizing activity against their corresponding variants
301 (Figure 5A). Among all three, the circRNA^{RBD-Delta} vaccine maintained sufficient neutralizing
302 activity against Omicron (Figure 5A), with an NT50 of $\sim 4.7 \times 10^3$, while the NT50 of the
303 circRNA^{RBD-Beta} against Omicron dropped below 5×10^2 (Figure 5A). Compared to the mRNA^{RBD-}
304 ^{Delta} vaccine, the circRNA^{RBD-Delta} vaccine elicited comparable neutralizing activity against both
305 Delta and Omicron variants for mouse sera collected 2 weeks after the boost (short-term) and 7
306 weeks after the boost (long-term) (Figures 5A-5C). Similar to the above observations (Figure 3M),
307 the circRNA^{RBD-Delta} vaccine also elicited a higher average proportion of neutralizing antibodies
308 against Omicron variant than the 1m Ψ -mRNA^{RBD-Delta} vaccine at both 2 weeks after the boost
309 (short-term) and 7 weeks after the boost (long-term) (Figures S6A-S6D), indicating the potential
310 superiority of the circRNA vaccine against the circulating variants of SARS-CoV-2.

311

312 **CircRNA^{RBD-Omicron} vaccine elicited neutralizing antibodies against Omicron**

313 We developed an Omicron-specific circRNA vaccine that expressed the trimeric RBD antigens of
314 the Omicron variant. Mice were immunized i.m. with 5 μ g or 10 μ g of circRNA^{RBD-Omicron} vaccines
315 twice at a 2-week interval. One week after the boost dose, the serum samples from immunized
316 mice were collected for the detection of specific antibodies. The circRNA^{RBD-Omicron} vaccine
317 induced Omicron spike-specific antibodies with the endpoint GMTs of $\sim 4.7 \times 10^4$ for the 5 μ g dose
318 and $\sim 2.2 \times 10^5$ for the 10 μ g dose (Figure 5D), yielding clear neutralizing activities against Omicron
319 with NT50 values of $\sim 2.5 \times 10^3$ for the 5 μ g dose and $\sim 8.6 \times 10^3$ for the 10 μ g dose (Figure 5E).
320 However, neutralizing activity could hardly be detected against the native strain or Delta variant
321 (Figures 5E and 5F).

322

323 **The third booster with the circRNA^{RBD-Delta} vaccine markedly elevated the neutralizing** 324 **antibodies against the current VOCs**

325 We next investigated the feasibility of circRNA vaccines as a booster. Mice immunized with two

326 doses of circRNA^{RBD-Delta} vaccines received a 3rd booster with circRNA^{RBD-Beta}, circRNA^{RBD-Delta}
327 or circRNA^{RBD-Omicron} vaccine at 7 weeks after the 2nd dose, followed by the assessment of
328 neutralizing activity at 1 week after boost (Figure 5G). Only circRNA^{RBD-Delta} effectively boosted
329 the neutralizing antibodies against both Delta (Figure 5H) and Omicron (Figure 5I). In contrast,
330 the 3rd boost with the circRNA^{RBD-Beta} or circRNA^{RBD-Omicron} vaccine failed to elevate the
331 neutralizing capability against Delta or Omicron (Figures 5H and 5I).

332 We then tested the 3rd booster with circRNA^{RBD} or circRNA^{RBD-Delta} vaccine in mice previously
333 immunized with 2-dose circRNA^{RBD} vaccines (Figure 5J). Both vaccines effectively boosted
334 neutralizing antibodies against both Delta (Figure 5K) and Omicron (Figure 5L). CircRNA^{RBD-Delta}
335 appeared to be a much better booster than circRNA^{RBD} against both Delta and Omicron variants,
336 which elevated the geometric mean NT50 from $\sim 4 \times 10^2$ to $\sim 3.2 \times 10^4$ against the Omicron (Figures
337 5K and 5L).

338 Taken together, these results suggest that circRNA^{RBD-Delta} might be a favorable choice for
339 vaccination to provide broad-spectrum protection against the current VOCs.

340

341 **CircRNA vaccine elicited potent neutralizing antibodies and Th1-biased immune responses** 342 **in rhesus macaques**

343 To further assess the immunogenicity of circRNA vaccine in nonhuman primates (NHPs), groups
344 of 2- to 4-year-old rhesus macaques were immunized i.m. with 20 μ g, 100 μ g or 500 μ g of
345 circRNA^{RBD} vaccines, 100 μ g of circRNA^{Ctrl}, or PBS control on days 0 and 21 (Figure 6A). The
346 specific antibodies were measured using the rhesus macaque plasma collected at 2 weeks after the
347 boost (Figure 6A). The IgG endpoint GMTs reached $\sim 2.1 \times 10^4$ (20 μ g), $\sim 1.6 \times 10^4$ (100 μ g dose)
348 and $\sim 7 \times 10^3$ (500 μ g dose) for circRNA^{RBD} vaccines, while circRNA^{Ctrl}- or PBS-immunized rhesus
349 macaques failed to induce RBD-specific antibodies (Figure 6B). The pseudovirus neutralization
350 assay showed NT50 values of ~ 180 for the 20 μ g dose, ~ 520 for the 100 μ g dose, and ~ 390 for the
351 500 μ g dose (Figure 6C). The authentic SARS-CoV-2 neutralization assay showed NT50 values
352 of ~ 80 for the 20 μ g dose, ~ 120 for the 100 μ g dose, and ~ 50 for the 500 μ g dose (Figures 6D and
353 6E).

354 We then performed a cross-neutralizing assay. Both the pseudotyped and authentic SARS-
355 CoV-2 neutralization assays showed that the circRNA^{RBD} vaccine-immunized rhesus macaque

356 plasma could effectively inhibit the corresponding native strain, while the Alpha, Delta and Beta
357 variants could also be inhibited, but with reduced activity, especially against the Beta variant
358 (Figures 6D and 6E).

359 Peripheral blood mononuclear cells (PBMCs) were collected on the day before challenge with
360 SARS-CoV-2. The RBD-specific T cell responses in rhesus macaques were measured using
361 PBMCs stimulated with the RBD peptide pools (Table S5). The ELISpot assay showed evident
362 IFN- γ and IL-2 responses, but nearly undetectable IL-4 in circRNA^{RBD}-immunized rhesus
363 macaques (Figure 6F), indicating a Th1-biased T cell immune response.

364

365 **CircRNA vaccine protected the rhesus macaques against SARS-CoV-2 infection**

366 Five weeks after the boost dose, the immunized rhesus macaques were challenged with 1×10^6 PFU
367 of the SARS-CoV-2 native strain as described previously (Vogel et al., 2021). The challenged
368 rhesus macaques were euthanized at 7 days post-infection (dpi), and the lung tissues underwent
369 viral load and histopathological assays. The RT-qPCR assay using primers targeting SARS-CoV-
370 2 genomic RNA (N gene) indicated that the rhesus macaques immunized with 100 μ g or 500 μ g
371 of circRNA^{RBD} vaccine were well protected as the viral genomic RNAs were reduced nearly 1000-
372 fold compared to the control groups (Figure 6G). To detect the actively replicative viral loads, we
373 performed qPCR using primers targeting SARS-CoV-2 subgenomic RNA (E gene) and found that
374 rhesus macaques immunized with circRNA^{RBD} at all three doses had nearly no detectable viral
375 subgenomic RNA in the lung tissues (Figure 6G).

376 Further histopathological examination demonstrated that circRNA^{RBD}-immunized rhesus
377 macaques of all doses were well protected because only very mild pneumonia was observed
378 (Figure 6H). In contrast, severe pneumonia was observed in the lungs of the two control groups,
379 as exemplified by local pulmonary septal thickening, moderate hemorrhage in the pulmonary
380 septals, a large number of scattered dust cells, and massive inflammatory cell infiltration (Figure
381 6H). The pathological scores further confirmed that circRNA^{RBD} immunization significantly
382 protected the rhesus macaques against COVID-19 (Figure 6I), likely resulting from a synergy
383 between the humoral immune responses and T cell responses by vaccination (Figure 6J).

384

385 **CircRNA vaccine did not cause clinical signs of illness in rhesus macaques**

386 To further evaluate the safety of circRNA vaccines in NHPs, physiological and biochemical
387 indicators were monitored. No severe clinical adverse effects were observed following the priming
388 or boost dose. CircRNA^{RBD} vaccines induced evident IL-6 and MCP-1 (Figures S7A and S7B),
389 while TNF- α , IL-1 β , and IFN- α were nearly undetectable (Figures S7C-S7E). The body
390 temperatures of both immunized rhesus macaques and controls were within the normal range after
391 prime and boost (Figure S7F). None of the challenged macaques showed clinical signs of illness
392 (Figures S7G-S7K). Collectively, our study provides preliminary proof of safety for the circRNA
393 vaccination in NHPs.

394

395 **Expression of SARS-CoV-2 neutralizing antibodies via the circRNA platform**

396 In addition to vaccines, circRNAs could be repurposed for therapeutics when used to express other
397 proteins, antibodies or peptides. Here, we attempted to test the therapeutic potential of circRNAs
398 by expressing antibodies. It has been reported that SARS-CoV-2 neutralizing nanobodies or
399 hACE2 decoys can inhibit SARS-CoV-2 infection (Linsky et al., 2020; Schoof et al., 2020; Xiang
400 et al., 2020; Chan et al., 2020). This prompted us to leverage the circRNA platform to express
401 SARS-CoV-2 neutralizing nanobodies and hACE2 decoys (Figure 7A). Pseudovirus neutralization
402 assays showed that supernatants of HEK293T cells transfected with circRNA^{nAB} or circRNA^{hACE2}
403 ^{decoys} could effectively inhibit SARS-CoV-2 pseudovirus infection (Figure 7B).

404 Next, we tested neutralizing antibodies against the SARS-CoV-2 variants, Alpha and Beta. The
405 supernatants of circRNA^{nAB1-Tri} and circRNA^{nAB3-Tri} effectively blocked Alpha and D614G
406 pseudovirus infection (Figure 7C). However, both nanobodies showed markedly decreased
407 neutralizing activity against Beta variant (Figure 7C). The hACE2 decoys showed no inhibition
408 activity against Alpha and Beta variants (Figure 7C).

409

410 **DISCUSSION**

411 COVID-19 is still a fast-growing global health crisis with circulating SARS-CoV-2 variants evading
412 immunity from prior vaccination or viral infection, especially with the emerging Delta and
413 Omicron variants of concern (Karim and Karim; Muik et al., 2021; Wang et al., 2021a; Wang et
414 al., 2021b). Our study established a circular RNA vaccination strategy to elicit effective

415 neutralizing antibodies and T cell immune responses against SARS-CoV-2 and its emerging
416 variants.

417 As reported, most effective neutralizing antibodies recognize the RBD region of the spike
418 protein (Barnes et al., 2020; Cao et al., 2020; Du et al., 2020; Koenig et al., 2021; Schoof et al.,
419 2020; Xiang et al., 2020), and targeting the RBD may induce fewer non-neutralizing antibodies
420 (Huang et al., 2021; Laczko et al., 2020; Sahin et al., 2020; Tai et al., 2020; Zhang et al., 2020).
421 Given that RBD trimers bind to hACE2 better than their monomeric counterparts and have been
422 shown to enhance the humoral immune response (Bouwman et al., 2021; Routhu et al., 2021; Sahin
423 et al., 2020), we chose to express RBD trimers via circRNA as the immunogen. The circRNA-
424 encoded RBD trimers were functional and successfully induced potent neutralizing antibodies and
425 specific T cell responses against SARS-CoV-2 in both mice and rhesus macaques (Figures 2, 4
426 and 6).

427 mRNA vaccines based on the full-length spike protein (mRNA-1273 and BNT162b2) (Corbett
428 et al., 2020a; Corbett et al., 2020b; Vogel et al., 2021) or RBD elicit neutralizing antibodies and T
429 cell responses (Huang et al., 2021; Laczko et al., 2020; Sahin et al., 2020; Tai et al., 2020; Zhang
430 et al., 2020). In comparison with the mRNA vaccine, the circRNA vaccine elicited higher and
431 more durable immunogens, leading to distinct Th1-biased T cell immune responses from the
432 mRNA vaccine (Figures 3 and S3). Moreover, the circRNA^{RBD-Delta} vaccine induced a higher
433 average proportion of neutralizing antibodies against both Delta and Omicron variants than the
434 mRNA^{RBD-Delta} vaccine (Figures 3M and S6). We infer that the more durable antigen production
435 and distinct immunogenicity of circRNA vaccine (Figures 3A-3E) enabled the elicitation of higher
436 proportion of neutralizing antibodies and distinct Th1-skewed immune responses than the 1mΨ-
437 modified mRNA vaccine (Figures 3G-3M) by promoting and elongating the antibody affinity
438 maturation process in germinal centers after vaccination (Alameh et al., 2021; Liu et al., 2021a).

439 A recent preprint reported that vaccinees who received two doses of SARS-CoV-2 vaccine
440 exhibited enhanced neutralizing antibodies against Delta variant after infection with Omicron,
441 implying that an Omicron vaccine might provide broad-spectrum protection against other variants
442 (Khan et al., 2021). Our result argues against this possibility because our Omicron-specific vaccine
443 failed to cross protect against the Delta variant (Figures 5D-5F) or boost the two-dose Delta
444 vaccine (Figures 5H and 5I). In contrast, the circRNA^{RBD-Delta} vaccine appeared to produce

445 antigens possessing high immunogenicity and consequently elicit a high level of neutralizing
446 antibodies against Delta (Figures 2 and 3). Our Delta-specific vaccination could cross protect
447 against all other variants, including Omicron (Figures 2E, 5A, 5B and 5C), and could also be used
448 as an effective booster following two-dose original SARS-CoV-2 vaccines (Figures 5K and 5L).
449 It is hoped that further testing will show that the circRNA^{RBD-Delta} vaccine could be applied as an
450 effective booster for current major vaccines.

451 Currently, mRNA-1273 and BNT162b2 were widely administrated, both of which were
452 produced with complete replacement of uridine by 1-methylpseudouridine to reduce unwanted
453 immunogenicity (Corbett et al., 2020a; Corbett et al., 2020b; Kariko et al., 2005; Vogel et al.,
454 2021). In this study, no nucleotide modification was used for the circRNA vaccine. We found that
455 the immunogenicity of LNP-encapsulated circRNA^{RBD} was at a comparable level to that of LNP-
456 encapsulated 1m Ψ -mRNA^{RBD} in the cell culture (Figure 3E). Moreover, although our study was
457 not specifically designed for studying the safety of vaccines or drugs, it is worth noting that
458 circRNA vaccine did not cause clinical signs of illness or enhanced pathology in vaccinated non-
459 human primates, thereby opening avenues for the development of circRNA-based vaccines or
460 drugs (Figures 6 and S7). It will be interesting to see if nucleotide modifications can further
461 improve the therapeutic applicability of circRNAs in future studies, while currently it is technical
462 challenging because the 1m Ψ modification would disrupt IRES function (Wesselhoeft et al., 2019).

463 In this study, we also tested the therapeutic potential of circRNAs that encode SARS-CoV-2-
464 specific neutralizing nanobodies (Barnes et al., 2020; Cao et al., 2020; Du et al., 2020; Koenig et
465 al., 2021; Schoof et al., 2020; Xiang et al., 2020) or hACE2 decoys (Chan et al., 2020; Glasgow et
466 al., 2020), which could effectively neutralize the SARS-CoV-2 pseudovirus (Figure 7). Beyond
467 viral receptors, this circRNA expression platform holds the potential to become a therapeutic drug
468 encoding therapeutic antibodies *in vivo*, such as anti-PD1/PD-L1 antibodies (Boutros et al., 2016;
469 He and Xu, 2020). Unlike antibodies and protein drugs, circRNAs encode therapeutic antibodies
470 in the cytoplasm, allowing them to target intracellular targets such as TP53 (Sabapathy and Lane,
471 2018) and KRAS (Mukhopadhyay et al., 2021), bypassing the cytomembrane barrier.

472 In summary, circular RNA holds the potential to become an effective and safe platform for
473 vaccination against viral infection, including SARS-CoV-2 emerging variants, as well as a
474 therapeutic platform, owing to its specific properties.

475

476 Limitations of the study

477 The small numbers of rhesus macaques we used for the challenge experiments led to high
478 variations and large error bars in the evaluation of circRNA vaccines. The immunogenicity of IVT-
479 produced circRNAs is another potential concern (Chen et al., 2019; Liu et al., 2021b; Wesselhoeft
480 et al., 2019). While our study showed that circRNA vaccines did not cause any clinical signs of
481 illness in rhesus macaques, even at high doses (500 µg per rhesus macaque) (Figure 6), the safety
482 of circRNA vaccines awaits further investigation in NHPs and clinical trials. In the current study,
483 we observed that the circRNA vaccine outperformed the mRNA vaccine counterpart in several
484 aspects; however, more detailed and comprehensive comparisons need to be conducted in the
485 future. It is worth noting that the mRNA vaccine we used for the comparison study is different
486 from the two widely inoculated vaccines, mRNA-1273 and BNT162b2, both of which encode the
487 full-length spike antigens and were produced by different manufacturing processes, while the
488 mRNA vaccine in this study encoded the trimeric RBD of spike (Corbett et al., 2020a; Corbett et
489 al., 2020b; Vogel et al., 2021).

490

491 ACKNOWLEDGMENTS

492 We acknowledge Chen Dong and Xiaohu Wang (Tsinghua University) for providing fluorescent
493 dye-conjugated antibodies. We thank Junyu Xiao (Peking University) for providing purified
494 SARS-CoV-2 spike proteins and Jinghua Yan (Institute of Microbiology, Chinese Academy of
495 Sciences) for providing RBD peptide pools. We thank the Laboratory Animal Center of Peking
496 University for the maintenance of mice. We thank the HPLC Core at the National Center for
497 Protein Sciences at Peking University (Beijing), particularly H. Li and G. Li for their technical
498 help. We thank the flow cytometry Core at the National Center for Protein Sciences at Peking
499 University (Beijing), particularly H. Lv, Y. Guo, H. Yang, and F. Wang for their technical help.
500 This project was supported by funds from National Key R&D Program of China
501 (2020YFA0707800 to W.W., 2020YFA0707600 to Z.Z.); the Beijing Municipal Science &
502 Technology Commission (Z181100001318009); the National Science Foundation of China
503 (31930016); the Beijing Advanced Innovation Center for Genomics at Peking University and the
504 Peking-Tsinghua Center for Life Sciences (to W.W.); the National Science Foundation of China

505 (31870893); the National Major Science & Technology Project for Control and Prevention of
506 Major Infectious Diseases in China (2018ZX10301401 to Z.Z.), and the Fellowship of China
507 National Postdoctoral Program for Innovative Talents (BX20200010, to L.Q.).

508

509 **AUTHOR CONTRIBUTIONS**

510 W.W. conceived and supervised this project. W.W., L.Q., Z.Y. and Y.S. designed the experiments.
511 L.Q., Z.Y., Y.S., L.L., F.C., Y.X., Z.W. and H.T. performed the preparation of circRNA vaccines,
512 mouse vaccination experiments, detection experiments and data collection with the help of X.Z.,
513 F.T., C.W., A.Y., Y.C., Z.Z., X.S.X. and W.W. L.Q., Z.Y., Y.S., X.X. and X.D. performed the
514 SARS-CoV-2 Beta variant challenge experiments in mice and related detection experiments with
515 the help of Z.Z., L.G., J.W. and W.W. L.Q., Z.Y., Y.S. and S.L. performed the rhesus macaque
516 experiments and related detection experiments with the help of C.Y., C.T., Y.Y., W.Y., J.W., Y.Z.,
517 Q.H., X.P. and W.W. The VSV-based SARS-CoV-2 pseudovirus was produced by S.L., W.H.,
518 and Y.W. L.Q., Z.Y., Y.S., Z.Z. and W.W. wrote the manuscript with the help from all other
519 authors.

520

521 **DECLARATION OF INTERESTS**

522 Patents related to the data presented have been filed. W.W. is the founder of Therorna, Inc. The
523 other authors declare no competing interests.

524

525

526 Figure 1. Immunogenicity and protection of circRNA vaccines against SARS-CoV-2 in mice

527 (A) Schematic diagram of circRNA^{RBD} circularization by group I intron autocatalysis. SP, signal
528 peptide sequence of human tPA. Foldon, the trimerization domain from bacteriophage T4 fibritin.

529 The arrows indicate the design of primers for PCR analysis.

530 (B) Western blot showing the expression level of RBD in the supernatant of HEK293T or NIH3T3
531 cells transfected with circRNA^{RBD}. The circRNA^{EGFP} and linear RNA precursor were used as
532 controls.

533 (C) Western blot result under reducing conditions (with DTT) or nonreducing conditions (without
534 DTT).

535 (D) Measurement of the concentration of RBD in the supernatant of HEK293T cells by ELISA.

536 (E) Competitive inhibition assay of SARS-CoV-2 pseudovirus infection by the circRNA^{RBD}-
537 translated RBD antigens.

538 (F) Schematic representation of the LNP-circRNA complex.

539 (G) Representative intensity-size graph of LNP-circRNA^{RBD} by the dynamic light scattering
540 method.

541 (H) Schematic diagram of the circRNA^{RBD} vaccination and antibody analysis in BALB/c mice.

542 (I) Measurement of the IgG antibody endpoint GMTs elicited by the circRNA^{RBD} vaccine.

543 (J) Measurement of the NT50 of LNP-circRNA^{RBD}-immunized mouse sera using pseudoviruses.

544 (K) Neutralization assay of SARS-CoV-2 authentic virus with the sera of mice immunized with
545 circRNA^{RBD} vaccine. The serum samples were collected at 5 weeks after the boost.

546 (L) Measurement of the SARS-CoV-2 (Beta) specific IgG endpoint GMTs elicited by the
547 circRNA^{RBD-Beta} vaccine.

548 (M and N) Sigmoidal curve diagram of the neutralization of VSV-based D614G, Alpha or Beta
549 pseudovirus with the sera of mice immunized with circRNA^{RBD} (M) or circRNA^{RBD-Beta} (N). The
550 sera were collected 1 week after the boost.

551 (O and P) Neutralization assay of SARS-CoV-2 Beta (O) or D614G (P) authentic virus with the
552 serum of mice immunized with circRNA^{RBD-Beta} vaccine.

553 (Q) Measurement of the viral loads in the mouse lung tissues. The SARS-CoV-2 RNA copies were
554 normalized to *GAPDH*.

555 (R) Measurement of the SARS-CoV-2 RBD-Beta-specific IgG endpoint GMTs.

556 (S) Sigmoidal curve diagram of the inhibition rate by sera from immunized mice with surrogate
 557 virus neutralization assay. In (R and S), the sera were collected 3 days before challenge.

558 (T) Viral loads in the lung tissues of challenged mice.

559 (U) The weight change of immunized or placebo mice after challenge.

560 (V) Measurement of the neutralizing activity of sera from mice immunized with circRNA^{RBD-Beta}
 561 vaccine. The circRNAs were encapsulated with LNPs (Precision Nanosystems) instead of the lab-
 562 prepared LNPs.

563 In (D and E), data were shown as the mean \pm S.E.M. (n = 2 or 3). In (I, J, K, L, O, P and R), data
 564 are shown as the geometric mean \pm geometric S.D. (n = 3~6). In (M, N, Q, S, T, U and V), data
 565 are shown as the mean \pm S.E.M. (n = 3~7). Each symbol represents an individual mouse. Unpaired
 566 two-sided Student's *t* test was performed for comparison as indicated.

567 See also Figures S1 and S2.

568

569 **Figure 2. Humoral immune responses elicited by circRNA^{RBD-Delta} vaccines in mice**

570 (A) Measurement of the SARS-CoV-2 Delta specific IgG endpoint GMTs elicited by circRNA^{RBD-}
 571 ^{Delta} vaccine generated by group I intron.

572 (B) Measurement of the SARS-CoV-2 Delta specific IgG endpoint GMTs elicited by circRNA^{RBD-}
 573 ^{Delta} vaccine generated by T4 RNA ligases.

574 (C) Neutralization assay of VSV-based SARS-CoV-2 (Delta) pseudovirus with the sera of mice
 575 immunized with circRNA^{RBD-Delta} vaccines.

576 (D and E) Sigmoidal curve diagram of the neutralization assay.

577 In (A-C), data are shown as the geometric mean \pm geometric S.D. (n = 5), and each symbol
 578 represents an individual mouse. In (D and E), data are shown as the mean \pm S.E.M. (n = 5).

579

580 **Figure 3. CircRNA vaccine elicited higher average proportions of neutralizing antibodies**
 581 **and distinct Th1-biased T cell immune responses than mRNA vaccine**

582 (A) Comparison of the antigen expression levels of circRNA^{RBD-Delta}, 1m Ψ -mRNA^{RBD-Delta} and
 583 nonmodified mRNA^{RBD-Delta} through Lipofectamine MessengerMax transfection in HEK293T
 584 cells.

585 (B) The dynamic change in RNA levels in (A).

586 (C) The antigen expression levels of LNP-circRNA^{RBD-Delta}, LNP-1mΨ-mRNA^{RBD-Delta} and LNP-
 587 nonmodified-mRNA^{RBD-Delta} in HEK293T cells. In (A-C), data are shown as the mean ± S.E.M. (n
 588 = 3).

589 (D) Western blot showing the expression level of RBD in the supernatant of HEK293T cells
 590 transfected with circRNA^{RBD}.

591 (E) The mRNA abundance of cytokines (MCP-1, IL-6, IP-10, TNF-α, IFN-α and RANTES)
 592 induced by circRNA^{RBD-Delta}, 1mΨ-mRNA^{RBD-Delta}, unmodified-mRNA^{RBD-Delta} via RT-qPCR
 593 analysis in HEK293T cells. The circRNA, 1mΨ-mRNA or unmodified-mRNA was delivered into
 594 HEK293T cells via MessengerMax or LNP. The mRNA levels were normalized by *GAPDH*. The
 595 mRNA fold changes were normalized using the untreated HEK293T cells. Data were shown as
 596 the mean ± SEM. (n = 2 or 3).

597 (F) Measurement of the RBD-Delta-specific IgG endpoint GMTs in mice.

598 (G) Measurement of RBD-Delta-specific IgG1/IgG2a/IgG2c endpoint GMTs in mice. In (F and
 599 G), data are shown as the geometric mean ± geometric S.D. (n = 11~12).

600 (H) Measurement of the specific IgG2a/IgG1, IgG2c/IgG1 and (IgG2a + IgG2c)/IgG1 ratios.

601 (I-L) Sigmoidal curve diagram of neutralization rate of VSV-based SARS-CoV-2 (Delta)
 602 pseudovirus with the sera from mice immunized with 0.5 μg (I), 2.5 μg (J), 5 μg (K) or 10 μg (L)
 603 of circRNA or 1mΨ-mRNA vaccines.

604 (M) The ratio of (neutralizing Ab)/(binding Ab) elicited by 0.5 μg, 2.5 μg, 5 μg or 10 μg of the
 605 circRNA or 1mΨ-mRNA vaccine. The ratio of (NT50)/(Endpoint GMT) of each mouse was
 606 calculated. In (H-M), data are shown as the mean ± S.E.M. (n = 10~12).

607 Unpaired two-sided Student's *t* test was performed for comparison as indicated in the figures, **p*
 608 < 0.05; ***p* < 0.01; ****p* < 0.001; *****p* < 0.0001; ns, not significant. Each symbol represents an
 609 individual mouse.

610 See also Figure S3.

611

612 **Figure 4. T cell immune responses elicited by SARS-CoV-2 circRNA^{RBD-Delta} or mRNA^{RBD-}**
 613 **Delta vaccines in mice**

614 (A-C) FACS analysis results showing the percentages of CD8⁺ Tem cells secreting IFN-γ (A), IL-
 615 2 (B), or TNF-α (C) after stimulation with RBD-Delta peptide pools.

616 (D-G) FACS analysis results showing the percentages of CD4⁺ Tem cells secreting IFN-γ (D), IL-

617 2 (E), TNF- α (F) or IL-4 (G) after stimulation. Empty LNP was used as the control. In (A-G), data
618 are presented as the mean \pm S.E.M. (n = 3 or 4), and each symbol represents an individual mouse.
619 Paired Student's *t* test was performed for comparison between the peptide pool-stimulated group
620 and un-stimulated group as indicated; unpaired two-sided Student's *t* test was performed for
621 comparison between circRNA^{RBD-Delta} vaccines and mRNA^{RBD-Delta} vaccines as indicated; **p* <
622 0.05; ***p* < 0.01; ****p* < 0.001; *****p* < 0.0001; ns, not significant.
623 See also Figures S4 and S5.

624

625 **Figure 5. CircRNA^{RBD-Delta} vaccine elicited high levels of neutralizing antibodies against both**
626 **the Delta and Omicron variants**

627 (A) Neutralization assay of VSV-based SARS-CoV-2 pseudovirus with the sera of immunized
628 mice.

629 (B and C) Neutralization assay of VSV-based SARS-CoV-2 pseudovirus with the sera of mice
630 immunized with 10 μ g (B) or 5 μ g (C) of circRNA or mRNA vaccines.

631 (D) Measuring the Omicron-spike-specific IgG endpoint GMTs of circRNA^{RBD-Omicron}-immunized
632 mouse sera.

633 (E) Measurement of the NT50 of LNP-circRNA^{RBD-Omicron}-immunized mouse sera using VSV-
634 based pseudoviruses. The serum samples were collected at 1 week after the boost dose. In (A-E),
635 data are shown as the geometric mean \pm geometric S.D. (n = 4 or 5).

636 (F) Sigmoidal curve diagram of the neutralization assay in (E). Data are shown as the mean \pm
637 S.E.M. (n = 4 or 5).

638 (G) Schematic diagram of the circRNA boost and antibody detection in mice receiving two-dose
639 prior circRNA^{RBD-Delta} vaccine.

640 (H and I) Measurement of the NT50 value of mouse sera boosted with circRNA vaccine (5 μ g)
641 after receiving two-dose circRNA^{RBD-Delta} vaccine (5 μ g) using VSV-based pseudoviruses of Delta
642 (H) or Omicron (I).

643 (J) Schematic diagram of the circRNA vaccination and antibody detection in mice receiving two-
644 dose of circRNA^{RBD} vaccine.

645 (K and L) Measurement of the NT50 value of mouse sera boosted with circRNA vaccine (20 μ g)
646 after receiving two-dose circRNA^{RBD} vaccine (20 μ g) using VSV-based pseudoviruses of Delta
647 (K) or Omicron (L).

648 In (B and C), unpaired two-sided Student's *t*-test was performed for comparison as indicated. In
649 (H, I, K, and L), paired Student's *t* test was performed for comparison as indicated. Each symbol
650 represents an individual mouse.

651 See also Figure S6.

652

653 **Figure 6. CircRNA vaccine elicits immunogenicity and protection against SARS-CoV-2**
654 **infection in rhesus macaques**

655 (A) Schematic diagram of the circRNA^{RBD} vaccination in rhesus macaques.

656 (B) Measurement of the SARS-CoV-2 RBD-specific IgG endpoint GMTs of the plasma from the
657 rhesus macaques immunized with circRNA^{RBD} vaccine, or circRNA^{Ctrl} (circRNA without the
658 RBD-encoding sequence) or PBS control.

659 (C) Measurement of the NT50 of the plasma of immunized rhesus macaques.

660 (D) Sigmoidal curve diagram of neutralization rate of VSV-based SARS-CoV-2 native, Alpha,
661 Beta and Delta pseudoviruses using the plasma of immunized rhesus macaques.

662 (E) Neutralization assay of authentic SARS-CoV-2 native, Alpha, Beta and Delta viruses using
663 the plasma of immunized rhesus macaques. Data are shown as the geometric mean \pm geometric
664 S.D. ($n = 4$).

665 (F) ELISpot assay measurement of the SARS-CoV-2 RBD-specific IFN- γ , IL-2 and IL-4 responses
666 of PBMCs from rhesus macaques immunized with circRNA vaccines. Data are shown as the mean
667 \pm S.E.M. ($n \geq 2$).

668 (G) Measurement of the viral loads (N gene) and subgenome RNA loads (E gene) in the lung
669 tissues of challenged rhesus macaques. Data are shown as the mean \pm S.E.M. ($n = 4$).

670 (H) HE staining of pathological sections using the lung tissues from immunized rhesus macaques
671 at 7 days after challenge.

672 (I) Pathological score of pneumonia based on the lung tissues from immunized rhesus macaques
673 at 7 days after challenge. The data are shown as the mean \pm S.E.M. ($n = 4$).

674 (J) Correlation of the B cell response, T cell response and pathological score in each immunized
675 rhesus macaque. Each symbol represents an individual macaque and symbol of the same rhesus
676 macaque is connected by line. B cell responses are shown by neutralizing antibody production as
677 a value of NT50 against authentic SARS-CoV-2 virus. T cell responses are shown as spots per 10^6
678 PBMCs detected in an IFN- γ and IL-2 ELISpot assay. Pathological scores are the same as in (I).

679 In (B, C and E), data are shown as the geometric mean \pm geometric S.D. ($n = 4$). In (D, F, G and
 680 D), data are shown as the mean \pm S.E.M. ($n = 2\sim 4$). Unpaired two-sided Student's t test was
 681 performed for comparison as indicated in the figures; $*p < 0.05$; $**p < 0.01$; $***p < 0.001$; $****p$
 682 < 0.0001 ; ns, not significant. Each symbol represents an individual rhesus macaque.

683 See also Figure S7.

684

685 **Figure 7. Expression of SARS-CoV-2 neutralizing nanobodies or hACE2 decoys via a**
 686 **circRNA platform**

687 (A) Schematic diagram of circRNA^{nAB} or circRNA^{hACE2 decoys} circularization by group I intron.

688 (B) Lentivirus-based pseudovirus neutralization assay with the supernatant from cells transfected
 689 with circRNA encoding nAB1, nAB1-Tri, nAB2, nAB2-Tri, nAB3 and nAB3-Tri or ACE2 decoys.
 690 The nAB1-Tri, nAB2-Tri and nAB3-Tri represent the trimers of nAB1, nAB2 and nAB3,
 691 respectively. The luciferase value was normalized to that of the circRNA^{EGFP} control.

692 (C) Sigmoidal curve diagram of neutralization of VSV-based SARS-CoV-2 D614G, Alpha or Beta
 693 pseudovirus using the supernatant of cells transfected with nAB1-Tri, nAB3-Tri or ACE2 decoys
 694 encoded by the corresponding circRNAs.

695 Data are shown as the mean \pm S.E.M. ($n = 2$ or 3).

696

697 **Figure S1. Optimization of the group I intron-based circRNA production approach and**
 698 **manufacturing of high-purity circRNAs via HPLC, Related to Figure 1**

699 (A) Agarose-gel RNA electrophoresis to test the effects of T7 RNA polymerase, rNTP or reaction
 700 time of *in vitro* transcription on the circularization efficiency of Anabaena group I-based
 701 circRNA^{RBD} production.

702 (B) HPLC chromatogram of circRNA^{RBD} via an Agilent 1260 HPLC instrument.

703 (C) Agarose-gel RNA electrophoresis of the collected fractions in (B).

704 (D) HPLC chromatogram of circRNA^{RBD} via Thermo UltiMate 3000 HPLC at the manufacturing
 705 level. The latter half of the main peak was collected to produce high-purity circRNA^{RBD}.

706 (E) Agarose-gel RNA electrophoresis results for the linear RNA precursor, unpurified circRNA^{RBD}
 707 and purified circRNA^{RBD}. The linear precursor was generated by mutating the 3' intron of the
 708 circRNA precursor as reference band in electrophoresis.

709 (F) Agarose-gel electrophoresis result of nicked RNA^{RBD} and circRNA^{RBD} treated with RNase R
710 for 5 min or 15 min. Nicked RNA^{RBD}, IVT-produced linear RNAs (share the same length and
711 sequence to circRNA^{RBD}.

712 (G) Formaldehyde-agarose denaturing gel electrophoresis of linear precursor RNAs, nicked
713 RNA^{RBD} and circRNA^{RBD}. Linear precursor and nicked RNA^{RBD} served as the reference bands in
714 electrophoresis.

715 (H) Urea-PAGE denaturing gel electrophoresis of linear precursor RNAs, nicked RNA^{RBD} and
716 circRNA^{RBD}. The time of Urea-PAGE denaturing gel electrophoresis was about 3 hr using Urea-
717 PAGE denaturing gels (Thermo).

718 (I) Measurement of the purity of circRNA^{RBD} with gray scan and integral calculus analysis.

719 (J) Agarose gel electrophoresis result of PCR analysis. Linear RNA precursor and circRNA^{RBD}
720 were reverse transcribed to cDNA, followed by PCR amplification with the specific primers shown
721 in Figure 1A.

722 (K) Sanger sequencing result of the PCR products in (J).

723 (L) Schematic diagram of RNase H assay. Linear precursor, nicked RNA^{RBD} or circRNA^{RBD} was
724 incubated with RNase H and a 15-nt ssDNA antisense probe (complementary to the above three
725 kind of RNAs) or 15-nt ssDNA sense probe (complementary to the antisense probe).

726 (M) Agarose gel electrophoresis of linear precursor RNAs, nicked RNA^{RBD} and circRNA^{RBD} after
727 the RNase H incubation reactions.

728

729 **Figure S2. Expression of SARS-CoV-2 RBD antigens with circular RNAs produced via T4**
730 **RNA ligase-based circularization, Related to Figure 1**

731 (A) Schematic diagram of circRNA^{RBD} circularization by T4 RNA ligase. SP, signal peptide
732 sequence of human tPA protein. Foldon, the trimerization domain from bacteriophage T4 fibritin
733 protein. RBD, the receptor binding domain of the SARS-CoV-2 spike protein.

734 (B) Sanger sequencing result of the DNA products produced by divergent PCR.

735 (C) Western blot analysis showing the expression level of RBD antigens in the supernatant of
736 HEK293T cells transfected with circRNA^{RBD} circularized by the T4 RNA ligase. The circRNA^{EGFP}
737 and linear RNA precursor were used as controls.

738 (D) Quantitative ELISA measurement of the concentration of RBD antigens in the supernatant.

739 Data are shown as the mean \pm S.E.M. (n = 3).

740
741 **Figure S3. Measuring the expression level of RBD-Delta antigens under different storage**
742 **conditions and the specific IgG2a/IgG1, IgG2c/IgG1 and (IgG2a + IgG2c)/IgG1 ratios,**
743 **Related to Figure 3**

744 (A) Agarose-gel RNA electrophoresis of 1m Ψ -RNA^{RBD-Delta} and unmodified mRNA^{RBD-Delta}.
745 (B-D) Quantitative ELISA was used to measure the expression of RBD-Delta antigens in the
746 supernatant of HEK293T cells transfected with LNP-circRNA^{RBD-Delta}, LNP-1m Ψ mRNA^{RBD-Delta}
747 and LNP-nonmodified-mRNA^{RBD-Delta} and stored at 4 °C (B), 25 °C (C) or 37 °C (D). The LNP-
748 RNAs were stored at different temperatures and transfected at different time points. Data are
749 shown as the mean \pm S.E.M. (n = 3).
750 (E) Measurement of RBD-Delta-specific IgG1/IgG2a/IgG2c endpoint GMTs elicited by 0.5 μ g
751 of circRNA^{RBD-Delta} vaccine or 1m Ψ -mRNA^{RBD-Delta} vaccine in mice. Data are shown as the
752 geometric mean \pm geometric S.D. (n = 10 or 11), and each symbol represents an individual
753 mouse.
754 (F) Measurement of the specific IgG2a/IgG1, IgG2c/IgG1 and (IgG2a + IgG2c)/IgG1 ratios in
755 serum from mice immunized with 0.5 μ g of circRNA^{RBD-Delta} or 1m Ψ mRNA^{RBD-Delta}. Data are
756 shown as the mean \pm S.E.M. (n = 10 or 11), and each symbol represents an individual mouse.
757 Unpaired two-sided Student's *t* test was performed for comparison as indicated in the figures.

758
759 **Figure S4. Flow panel and gating strategy to quantify SARS-CoV-2-RBD-specific T cells in**
760 **mice, Related to Figure 4**

761 (A) The plots show the gating strategy of single and viable T cells in spleenocytes. CD4⁺ or CD8⁺
762 Tem cells (CD44⁺CD62L⁻) were further analyzed to detect the expression of cytokines stimulated
763 by corresponding RBD-Delta peptide pools.
764 (B and C) Represented unvaccinated and vaccinated cohorts are shown for specific CD4⁺ T cell
765 responses (B) and CD8⁺ T cell responses (C).

766
767 **Figure S5. The ELISA results showing the cytokine levels in the supernatants of peptide**
768 **pool-stimulated splenocytes, Related to Figure 4**

769 (A-D) Measurement of the level of IFN- γ (A), IL-2 (B), TNF- α (C) or IL-4 (D) in the supernatants
770 of peptide pool-stimulated splenocytes with ELISA. The data were shown as the geometric mean
771 \pm geometric S.D. (n = 3 or 4), and each symbol represents an individual mouse. Unpaired two-

772 sided Student's *t*-test was performed for the comparison as indicated in the figures; **p* < 0.05; ***p*
773 < 0.01; ****p* < 0.001; *****p* < 0.0001; ns, not significant.

774

775 **Figure S6. The circRNA^{RBD-Delta} vaccine elicited a high level of neutralizing antibodies**
776 **against the Omicron variant, Related to Figure 5**

777 (A and B) Measurement of the ratio of (neutralizing antibodies)/(binding antibodies) elicited by
778 10 μg (A) or 5 μg (B) of circRNA^{RBD-Delta} vaccine or 1mΨ-mRNA^{RBD-Delta} vaccine in sera collected
779 2 weeks after the boost. The ratio of (NT50)/(endpoint GMT) of each mouse was calculated.

780 (C and D) Measurement of the ratio of (neutralizing antibodies)/(binding antibodies) elicited by
781 10 μg (C) or 5 μg (D) of circRNA^{RBD-Delta} vaccine or 1mΨ-mRNA^{RBD-Delta} vaccine with the sera
782 collected 7 weeks after the boost. The ratio of (NT50)/(endpoint GMT) of each mouse was
783 calculated. In (A-D), data are presented as the mean ± S.E.M. (n = 4~6), and each symbol
784 represents an individual mouse. The unpaired two-sided Student's *t* test was performed for
785 comparison as indicated in the figures.

786

787 **Figure S7. CircRNA vaccine caused no obvious clinical signs of illness in rhesus macaques,**
788 **Related to Figure 6**

789 (A-E) Measurement of the IL-6 (A), MCP1 (B), TNF-α (C), IL-1β (D) and IFN-α (E) level in the
790 plasma of immunized rhesus macaques.

791 (F) Monitoring the body temperature of rhesus macaques. Body temperature was monitored within
792 three days after the prime and boost doses. In (A-F), data are shown as the mean ± S.E.M. (n = 4).

793 (G-K) The body weight (G), temperature (H), heart rate (I), oxygen saturation (J), and respiratory
794 rate (K) were monitored after challenge with SARS-CoV-2. Data are shown as the mean ± S.E.M.

795 (n = 4).

796

797

798 **STAR★METHODS**

799 Detailed methods are provided in the online version of this paper and include the following:

- 800 • **KEY RESOURCES TABLE**
- 801 • **RESOURCE AVAILABILITY**
 - 802 ○ Lead Contact
 - 803 ○ Materials Availability
 - 804 ○ Data and Code Availability
- 805 • **EXPERIMENTAL MODEL AND SUBJECT DETAILS**
 - 806 ○ Animals and ethics statement
 - 807 ○ Cells and viruses
- 808 • **METHOD DETAILS**
 - 809 ○ Plasmid construction
 - 810 ○ Production and purification of circRNA
 - 811 ○ Production and purification of mRNA
 - 812 ○ RNase R cleavage assay
 - 813 ○ RNase H cleavage assay
 - 814 ○ CircRNA transfection *in vitro*
 - 815 ○ LNP encapsulation of circRNA
 - 816 ○ Quantitative determination of SARS-CoV-2 spike RBD expression *in vitro*
 - 817 ○ Mouse vaccination and serum collection
 - 818 ○ Antibody endpoint GMT measurement with ELISA
 - 819 ○ SARS-CoV-2 surrogate virus neutralization assay
 - 820 ○ Pseudovirus-based neutralization assay
 - 821 ○ Authentic SARS-CoV-2 NT50 assay
 - 822 ○ Mouse challenge experiments
 - 823 ○ Quantification of viral load in mice
 - 824 ○ T cell flow cytometry analysis
 - 825 ○ Rhesus macaque vaccination and plasma collection
 - 826 ○ ELISpot assay
 - 827 ○ SARS-CoV-2 challenge in rhesus macaques
 - 828 ○ Histopathology

829 ○ Cytokine analysis

830 • **QUANTIFICATION AND STATISTICAL ANALYSIS**

831

832 **SUPPLEMENTAL INFORMATION**

833 Supplemental information can be found online.

834

835

836

Journal Pre-proof

837 STAR★METHODS

838 KEY RESOURCES TABLE

REAGENT or RESOURCE	SOURCE	IDENTIFIER
Antibodies		
SARS-CoV-2 Spike RBD Rabbit pAb	ABclonal	Cat#A20135
Mouse monoclonal GFP antibody	Beyotime	Cat#AG281
Anti- β -Tubulin Mouse Monoclonal Antibody	Cwbio	Cat#CW0098M
Anti-Mouse IgG-Peroxidase antibody in rabbit	Merck	Cat#A9044
HRP-Monoclonal Mouse Anti-Monkey IgG	Immunoway	Cat#RS030204
Goat Anti-Mouse IgG1 (HRP)	Abcam	Cat#ab97240
Goat Anti-Mouse IgG2a (HRP)	Abcam	Cat#ab97245
Goat Anti-Mouse IgG2c (HRP)	Abcam	Cat#ab97255
Anti-Mouse CD3 Monoclonal Antibody, BV650	BioLegend	Cat#100229
Anti-Mouse CD4 Monoclonal Antibody, BV785	BioLegend	Cat#100552
Anti-Mouse CD8 Monoclonal Antibody, APC/ Cyanine7	BioLegend	Cat#100714
Anti-Mouse CD44 Monoclonal Antibody, FITC	BioLegend	Cat#103006
Anti-Mouse CD62L Monoclonal Antibody, BV711	BioLegend	Cat#104445
Anti-Mouse IFN- γ Monoclonal Antibody, APC	BioLegend	Cat#505810
Anti-Mouse IL-2 Monoclonal Antibody, AF700	BioLegend	Cat#503818
Anti-Mouse TNF- α Monoclonal Antibody, PE/Cyanine7	BioLegend	Cat#506324
Anti-Mouse IL-4 Monoclonal Antibody, PE	BioLegend	Cat#504104
Virus strains		
Lenti-based SARS-CoV-2 pseudovirus	This paper	N/A
Authentic SARS-CoV-2 virus	This paper	N/A
VSV-based SARS-CoV-2 pseudovirus	Institute for Biological Product Control, National Institutes for Food and Drug Control (NIFDC)	N/A
Chemicals, peptides, and recombinant proteins		
Lipofectamine MessengerMax	Thermo Fisher Scientific	Cat#LMRNA003
SARS-CoV-2 B.1.1.529 (Omicron) S1+S2 trimer Protein (ECD, His Tag)	Sino Biological	Cat#40589-V08H26
SARS-CoV-2 (2019-nCoV) Spike RBD-His Recombinant Protein	Sino Biological	Cat#40592-V08H
SARS-CoV-2 (2019-nCoV) Spike RBD (K417N, E484K, N501Y)-His Recombinant Protein	Sino Biological	Cat#40592-V08H85
SARS-CoV-2 Spike RBD (L452R, T478K) Protein (His Tag)	Sino Biological	Cat#40592-V08H90
SARS-CoV-2 B.1.1.529 (Omicron) Spike RBD Protein (His Tag)	Sino Biological	Cat#40592- V08H121
X tremeGENE HP DNA Transfection Reagent	Roche	Cat#6366236001
BRITELITE PLUS	Perkinelmer	Cat#6066769
Dulbecco's Modified Eagle Medium	Coring	Cat#10-013-CV
Fetal Bovine Serum	Biological Industries	Cat#C04001-500
Bovine Serum Albumin	Merck	Cat#B2064
ELISA Stop Solution	Bioss	Cat#C04-01003

1-Step Ultra TMB ELISA substrates	Thermo Fisher Scientific	Cat#34029
ELISA Washing Buffer (10x)	Bioss	Cat#C04-01004
RPMI 1640	Thermo Fisher Scientific	Cat#C11875500BT
eBioscience Cell Stimulation Cocktail (500x)	Thermo Fisher Scientific	Cat#00-4970-93
AIM-V Medium	Thermo Fisher Scientific	Cat#12055091
Phytohemagglutinin	Merck	Cat#L1668
PmeI	New England Biolabs	Cat#R0560L
DNase I	New England Biolabs	Cat#M0303L
RNase R	Epicentre	Cat#RNR07250
RNase H	New England Biolabs	Cat#M0297
T4 RNA Ligase 2	New England Biolabs	Cat#M0239
Quick CIP	New England Biolabs	Cat#M0525L
TB Green Premix Ex Taq II	TaKaRa	Cat#RR820A
HindIII-HF	New England Biolabs	Cat#R3104L
RNase Inhibitor, Murine	APEX BIO	Cat#K1046
m7G(5')ppp(5')G RNA Cap Structure Analog	New England Biolabs	Cat#S1404S
Critical commercial assays		
SARS-CoV-2 Spike RBD Protein ELISA kit	ABclonal	Cat#RK04135
SARS-CoV-2 Surrogate Virus Neutralization Test Kit	GenScript	Cat#L00847A
Nano-Glo Luciferase Assay System	Promega	Cat#N1110
Monkey IFN- γ ELISpot PLUS kit (HRP)	Mabtech	Cat#3421M-4HPW-2
Monkey IL-2 ELISpot PLUS kit (HRP)	Mabtech	Cat#3445M-4HPW-2
Monkey IL-4 T cell ELISPOT kit	U-CyTech	Cat#CT128-PR5
Monkey IL-6 ELISA kit	Abcam	Cat#ab242233
Monkey MCP-1 ELISA kit	Cloud-clone	Cat#SEA087Si96T
Monkey TNF- α ELISA kit	Abcam	Cat#ab252354
Monkey IL-1 β ELISA kit	Cloud-clone	Cat#SEA563Si96T
Monkey IFN- α ELISA kit	Chenglin	Cat#AD0081Mk
DNA Clean & Concentrator	Zymo Research	Cat#D4034
T7 High Yield RNA Synthesis Kit	New England Biolabs	Cat#E2040S
RNA Clean & Concentrator	Zymo Research	Cat#R1017
Monarch [®] RNA Cleanup Kit	New England Biolabs	Cat#T2040L
Zombie Aqua Fixable Viability Kit	BioLegend	Cat#423102
Fixation/Permeabilization Solution Kit with BD GolgiStop	Becton, Dickinson and Company	Cat#554715
Quant-it RiboGreen RNA Assay Kit	Thermo Fisher Scientific	Cat#R11490
Experimental models: Cell lines		
Human: HEK293T	This paper	N/A
Mouse: NIH3T3	This paper	N/A
Human: Huh-7	This paper	N/A
Human: HEK293T-hACE2	Biodragon	Cat#BDAA0039
Human: A549-hACE2	This paper	N/A
Experimental models: Organisms/strains		
Mouse: BALB/c	Beijing Vital River Laboratory Animal Technology Co., Ltd	N/A

Rhesus macaque	National Kunming High-level Biosafety Primate Research Center, Institute of Medical Biology, Chinese Academy of Medical Sciences and Peking Union Medical College, Yunnan China.	N/A
Recombinant DNA		
pcircRNA backbone	This paper	N/A
psPAX2	Ou et al., 2020	N/A
pSpike	Ou et al., 2020	N/A
pLenti-Luc-GFP	Ou et al., 2020	N/A
Software and algorithms		
GraphPad Prism Version 8.0	Graphpad	https://www.graphpad.com/
Image Lab	Bio-Rad	N/A
FlowJo	BD	N/A

839

840 **RESOURCE AVAILABILITY**841 **Lead Contact**

842 Further information and requests for resources and reagents should be directed to and will be
843 fulfilled by the Lead Contact, wswei@pku.edu.cn (W.W.).

844

845 **Material Availability**

846 All unique reagents generated in this study, such as circRNA, mRNA and cell lines are available
847 from the Lead Contact with a completed Material Transfer Agreement.

848

849 **Data and Code Availability**

850 All data and materials presented in this manuscript are available from the corresponding author
851 (W.W.) upon a reasonable request under a completed Material Transfer Agreement. This paper
852 does not report original code. Any additional information required to reanalyze the data reported
853 in this work paper is available from the Lead Contact upon request. Additional Supplemental Items
854 are available from Mendeley Data at <http://dx.doi.org/10.17632/vp2fskswfv.1>.

855

856 **EXPERIMENTAL MODEL AND SUBJECT DETAILS**857 **Animals and ethics statement**

858 The female BALB/c mice (6- to 8-week old) were ordered from Beijing Vital River Laboratory
859 Animal Technology Co., Ltd. All mice were bred and kept under specific pathogen-free (SPF)
860 conditions in the Laboratory Animal Center of Peking University. The animal experiments were
861 approved by Peking University Laboratory Animal Center (Beijing) and undertaken in accordance
862 with the National Institute of Health Guide for Care and Use of Laboratory Animals. All animal
863 experiments with SARS-CoV-2 challenge were conducted under animal biosafety level 3 (ABSL3)
864 facilities at the Institute of Pathogen Biology, Chinese Academy of Medical Sciences. All the
865 animal experiments with SARS-CoV-2 challenge were reviewed and approved by the Committee
866 on the Ethics of Animal Experiments of the Institute of Pathogen Biology, Chinese Academy of
867 Medical Sciences.

868 The 2- to 4-year-old male rhesus macaque experiments were performed in the animal biosafety
869 level 4 (ABSL-4) facility of the National Kunming High-level Biosafety Primate Research Center,
870 Yunnan, China. All animal procedures were approved by the Institutional Animal Care and Use
871 Committee of the Institute of Medical Biology, Chinese Academy of Medical Science.
872 Commercial monkey chow treats and fruit were provided daily by trained personnel.

873

874 **Cells and viruses**

875 HEK293T, NIH3T3 and Huh-7 cell lines were maintained in our laboratory. The HEK293T-
876 hACE2 cell line was ordered from Biodragon Inc. (#BDAA0039, Beijing, China). The A549-
877 hACE2 cell line was generated in our laboratory. These mammalian cell lines were cultured in
878 Dulbecco's Modified Eagle Medium (Corning, 10-013-CV) with 10% fetal bovine serum (FBS)
879 (BI), supplemented with 1% penicillin–streptomycin in 5% CO₂ incubator at 37 °C. The Huh-7
880 cells were cultured with the methods previously described methods (Cao et al., 2020).

881 The production of lentivirus-based SARS-CoV-2 pseudovirus and neutralization assays were
882 performed as described previously (Pinto et al., 2020). Briefly, the SARS-CoV-2 pseudovirus was
883 produced by cotransfecting plasmids psPAX2 (6 µg), pSpike (6 µg), and pLenti-Luc-GFP (6 µg)
884 into HEK293T cells using X tremeGENE HP DNA Transfection Reagent (Roche) according to
885 the manufacturer's instructions. Forty-eight hours after transfection, the supernatants containing
886 pseudovirus particles were harvested and filtered through a 0.22-µm sterilized membrane for the
887 neutralization assay as described below. The VSV-based pseudovirus of SARS-CoV-2 and its
888 variants were described previously (Cao et al., 2020; Du et al., 2020; Cao et al., 2021). Authentic

889 viruses were amplified from Vero-E6 cells and concentrated by an ultrafilter system via a 300 kD
890 module (Millipore). Amplified SARS-CoV-2 was confirmed via RT-PCR, sequencing and
891 transmission electronic microscopy, and titrated via plaque assay (10^6 PFU/ml).

892

893 **METHOD DETAILS**

894 **Plasmid construction**

895 The 5' homology arm sequence, 3' group I intron sequence, linker-1 sequence, IRES sequence,
896 linker-2 sequence, 5' group I intron sequence and 3' homology arm sequence were PCR amplified
897 and cloned into a plasmid backbone via the Gibson assembly strategy, generating the empty
898 pcircRNA-EV backbone. Then, the SARS-CoV-2 RBD antigen, EGFP, nanobody or hACE2-
899 decoy-coding sequence was PCR amplified and cloned into the pcircRNA-EV backbone, and the
900 corresponding pcircRNA plasmids were constructed for the following IVT reaction.

901

902 **Production and purification of circRNA**

903 The production of circRNAs was performed according to previous reports (Wesselhoeft et al.,
904 2018). Briefly, the circRNA precursors were synthesized via IVT from the linearized circRNA
905 plasmid templates with the HiScribe™ T7 High Yield RNA Synthesis Kit (New England Biolabs,
906 #E2040S). After IVT, the RNA products were treated with DNase I (New England Biolabs,
907 #M0303S) for 30 min to digest the DNA templates. After DNase I digestion, GTP was added to
908 the reaction at a final concentration of 2 mM, and then the reactions were incubated at 55 °C for
909 15 min to catalyze the cyclization of circRNAs. Then, the RNA was column purified with the
910 Monarch RNA Cleanup Kit (New England Biolabs, #T2040L). Then, the column-purified RNA
911 was heated at 65 °C for 3 min and cooled on ice. The reactions were treated with RNase R
912 (Epicenter, #RNR07250) at 37 °C for 15-30 min to further enrich the circRNAs. The RNase R-
913 treated RNA was column purified. For optimized IVT reaction, circRNAs were directly column
914 purified after IVT for further HPLC purification. The sequences of circRNAs produced via group
915 I intron were provided in Table S1.

916 We used split IRES strategy to produce circular RNAs by T4 RNA ligase 2 (NEB, #M0239).
917 To test the potential split sites in CVB3 IRES sequence, we analyzed the second structure of IRES.
918 After multiple tests and screens, we were able to determine the split site of CVB3 IRES at the 385th
919 nucleotide to allow T4 RNA ligase method for effective circularization. Then the circular RNA

920 precursors were produced via *in vitro* transcription (NEB, E2040S) with added Guanosine
921 monophosphates, and the RNA precursors were ligated by T4 RNA ligase 2 for 8 h at 25 °C.
922 Finally, the ligated circular products were treated with RNase R to remove the linear RNA
923 precursors. The sequences of circRNAs produced via T4 RNA ligases were provided in Table S2.

924 To further enrich the circRNAs, the purified RNase R-treated RNA was resolved with high-
925 performance liquid chromatography (Agilent HPLC1260) using a 4.6 × 300 mm size-exclusion
926 column with a particle size of 5 µm and pore size of 2000 Å (Sepax Technologies, #215980P-4630)
927 in RNase-free TE buffer (Thermo, #T11493). The circRNA-enriched fractions were collected and
928 then column purified. To further diminish the immunogenicity of the purified circRNAs, circRNAs
929 were heated at 65 °C for 3 min, cooled on ice and subsequently treated with Quick CIP phosphatase
930 (New England Biolabs, #M0525S). Finally, the circRNAs were column purified and concentrated
931 with the RNA Clean & Concentrator Kit (ZYMO, #R1018).

932

933 **Production and purification of mRNA**

934 The production of mRNAs referred to the manufacturer's instructions. Briefly, we produced the
935 mRNAs using the commercial HiScribe™ T7 High Yield RNA Synthesis Kit (NEB, #E2040S)
936 according to the manufacturer's instructions with the linearized plasmids containing the 5'-UTR,
937 RBD-coding region, 3'-UTR and -81-nt polyA elements. For 1mΨ-modified mRNA production,
938 the 1-Methylpseudouridine-5-Triphosphate (TriLink, #N-1081-10) was used instead of the
939 unmodified 5-Triphosphate for the production of 1mΨ-modified mRNA. The m7G(5')ppp(5')G
940 RNA Cap Structure Analog (NEB, #S1404) was used for cotranscriptional capping of mRNAs
941 according to the manufacturer's instructions. Final IVT products were column purified and
942 concentrated with the RNA Clean & Concentrator Kit (ZYMO, #R1018). The sequence of mRNA
943 was provided in Table S3.

944

945 **RNase H cleavage assay**

946 The purified circRNA^{RBD}, nicked linear RNA^{RBD} and linear precursor were incubated with RNase
947 H (NEB, M0297L). Site-specific cleavage was performed in reactions containing 500 ng of the
948 targeted RNAs, 50 pmol of the sense or antisense ssDNA probe and RNase H buffer in a total
949 volume of 18 µl. After incubation at 50 °C for 10 min, 2 µl of RNase H was added to the reaction

950 for 1 h at 37 °C. The sequence of the sense primer is 5'-TATTCTGTCCTCTAC-3', and the
951 sequence of the antisense primer is 5'-GTAGAGGACAGAATA-3'.

952

953 **RNase R cleavage assay**

954 The nicked RNA^{RBD} or circRNA^{RBD} was heated at 65 °C for 3 min before cooled on ice. The
955 RNase R (Epicentre, #RNR07250) was then added and incubated at 37 °C for 5 or 15 min. The
956 reactions were stopped by adding 2 × RNA loading dye (NEB, #B0363S), and RNAs were resolved
957 in agarose gel electrophoresis.

958

959 **CircRNA transfection *in vitro***

960 For circRNA transfection into HEK293T or NIH3T3 cells, 3×10⁵ cells per well were seeded in 12-
961 well plates. Two micrograms of circRNA was transfected into HEK293T or NIH3T3 cells using
962 Lipofectamine MessengerMax (Invitrogen, #LMRNA003) according to the manufacturer's
963 instructions. At 24-48 hr after transfection, the cell lysis and supernatant were collected for
964 subsequent detection.

965

966 **LNP encapsulation of circRNA**

967 The circRNAs were encapsulated with lipid nanoparticles (LNPs) according to a previously
968 described process (Ickenstein and Garidel, 2019). First, the circRNA was diluted with PNI
969 Formulation Buffer (Precision NanoSystems, #NWW0043) to a final concentration of 170 µg/ml.
970 Then, the lab-prepared or commercial LNP (Precision NanoSystems) were mixed with the
971 circRNA solution at the volume ratio of 1:3 through the Ignite NxGen Cartridge (Precision
972 NanoSystems, #NIT0002) using NanoAssemblr Ignite (Precision NanoSystems). Then the LNP-
973 circRNA formulations were diluted 40-fold with 1×PBS buffer (pH 7.2~7.4) and concentrated by
974 ultrafiltration with Amicon® Ultra Centrifugal Filter Unit (Millipore). The concentration and
975 encapsulation rate of circRNAs were measured by the Quant-it RiboGreen RNA Assay Kit
976 (Invitrogen, #R11490). The size of LNP-circRNA particles was measured using dynamic light
977 scattering on a Malvern Zetasizer Nano-ZS 300 (Malvern). Samples were irradiated with a red
978 laser, and scattered light was detected. The results were analyzed to obtain an autocorrelation
979 function using the software Zetasizer V7.13.

980

981 Quantitative determination of SARS-CoV-2 spike RBD expression *in vitro*

982 RBD expression in cell culture supernatants was quantified with a commercial SARS-CoV-2 spike
983 RBD Protein ELISA kit (ABclonal, #RK04135) according to the manufacturer's instructions. The
984 supernatants were diluted at proper ratio. Final concentrations of RBD were calculated based on
985 the linear standard curve of absorbance at 450 nm, using 630 nm as a reference. Briefly, the
986 detection wells were precoated with a monoclonal antibody specific for the spike RBD protein.
987 After incubation with samples or standards at 37 °C for two hours, samples unbound to
988 immobilized antibody were removed by washing steps. Then, RBD-specific antibodies were added
989 to the wells for a one-hour incubation at 37 °C. After washing, the HRP substrates and stop solution
990 were added, and the absorbance at 450 nm was measured using 630 nm as a reference.

991

992 Mouse vaccination and serum collection

993 For mouse vaccination, groups of 6- to 8-week-old female BALB/c mice were intramuscularly
994 immunized with LNP-circRNA^{RBD} or a placebo (LNP only) in 100 µl using a 1-ml sterile syringe,
995 and 2 or 3 weeks later, a second dose was administered to boost the immune responses. The sera
996 of immunized mice were collected to detect the SARS-CoV-2-specific IgG endpoint GMTs and
997 neutralizing antibodies as described below.

998

999 Antibody endpoint GMT measurement with ELISA

1000 All immunized mouse serum samples were heat-inactivated at 56 °C for 30 min before use. The
1001 SARS-CoV-2-specific IgG antibody endpoint GMT was measured by ELISA. Briefly, serial 3-
1002 fold dilutions (in 1% BSA) of heat-inactivated sera, starting at 1:100, were added to 96-well plates
1003 (100 µl/well; Costar) coated with recombinant SARS-CoV-2 spike or RBD antigens (Sino
1004 Biological) and blocked with 1% BSA for 60 min at 37 °C. Then, after three washes with wash
1005 buffer, horseradish peroxidase HRP-conjugated rabbit anti-mouse IgG (Sigma) diluted in 1% BSA
1006 at a 1:10,000 ratio was added to the plates and incubated at 37 °C for 30 min. Then, the plates were
1007 washed 3 times with wash buffer and added to TMB substrates (100 µl/well) followed by
1008 incubation for 15-20 min. Then, the ELISA stop buffer was added to the plates. Finally, the
1009 absorbance (450/630 nm) was measured with an Infinite M200 (TECAN). The IgG endpoint
1010 GMTs were defined as the dilution fold, which emitted an optical density exceeding 3x background
1011 (without serum but the secondary antibody was added).

1012

1013 SARS-CoV-2 surrogate virus neutralization assay

1014 The neutralizing activity of mouse serum samples was detected by a SARS-CoV-2 Surrogate Virus
1015 Neutralization Test Kit (L00847A, GenScript). Detections were performed according to the
1016 manufacturer's instructions. Serial 10-fold dilutions of heat-inactivated sera, starting at 1:10, were
1017 incubated with HRP-conjugated RBD solutions at 37 °C for half an hour, and then the mixtures
1018 were placed in 96-well plates precoated with human ACE2 (hACE2) proteins and incubated for
1019 15 min at 37 °C. After washing the TMB substrates, stop solution were added, and the absorbance
1020 (450/630 nm) was measured with an Infinite M200 (TECAN). The inhibition rates of serum
1021 samples were calculated according to the following formula. The 50% neutralization geometric
1022 mean titer (NT50) was determined using four-parameter nonlinear regression in Prism 8
1023 (GraphPad).

1024
$$\text{Inhibition rate} = (1 - \text{OD value of sample} / \text{OD value of negative control}) \times 100\%$$

1025

1026 Pseudovirus-based neutralization assay

1027 For the determination of the NT50 of immunized mouse serum, HEK293T-hACE2 cells were
1028 seeded in 96-well plates (50,000 cells/well) and incubated for approximately 24 hr until reaching
1029 over 90% confluence in preparation for pseudovirus infection. The mouse serum was diluted 3-
1030 fold, starting at 1:40, and incubated with the SARS-CoV-2 pseudovirus (MOI \approx 0.05) at 37 °C for
1031 60 min. DMEM without serum was used as the negative control group. Then, the supernatant of
1032 HEK293T-hACE2 cells was removed, and a mixture of serum and pseudovirus was added to each
1033 well. Thirty-six to 48 hr later, the luciferase activity, which reflects the degree of SARS-CoV-2
1034 pseudovirus transfection, was measured using the Nano-Glo Luciferase Assay System (Promega).
1035 The NT50 was defined as the fold dilution that achieved more than 50% inhibition of pseudovirus
1036 infection compared with the control group.

1037 The sera were serially diluted using complete DMEM as the culture medium in 96-well white
1038 plates for a total of six gradients, and then the virus solution with $\sim 1.3 \times 10^4$ TCID50 was added.
1039 Complete DMEM was used as the control group. After one hour of incubation in a 5% CO₂
1040 incubator at 37 °C, Huh7 cells (100 μ l/well) were added to the 96-well white plates, which were
1041 adjusted to a concentration of 2×10^5 cells/ml. After 24 h of incubation in a 5% CO₂ incubator at
1042 37 °C, the culture supernatant was aspirated gently to leave 100 μ l in each well, and then 100 μ l

1043 of luciferase substrate (PerkinElmer, #6066769) was added to each well for the detection of
1044 luminescence using an Infinite M200 (TECAN). Relative luciferase units (RLU) were normalized
1045 to the corresponding DMEM control group, and the NT50 was determined by four-parameter
1046 nonlinear regression in Prism (GraphPad).

1047 For the neutralization assay of circRNA^{nAB} or circRNA^{ACE2 decoys}, HEK293T-hACE2 cells were
1048 seeded in 96-well plates (50,000 cells/well) and incubated for approximately 24 hr until they
1049 reached over 90% confluence. The pseudoviruses were preincubated with the supernatant of the
1050 circRNA^{nAB}- or circRNA^{ACE2} decoy-transfected cells at 37 °C for 60 min and then added to cells
1051 in 96-well plates. Media were changed 24 hr after transduction. All cells were collected 48 hr after
1052 transduction. Luciferase activity was measured using the Nano-Glo Luciferase Assay System
1053 (Promega). The relative luminescence units were normalized to cells infected with the supernatant
1054 of cells transfected with circRNA^{EGFP}.

1055

1056 **Authentic SARS-CoV-2 NT50 assay**

1057 A549-hACE2 cells were seeded in 96-well plates (20,000 cells/well) and incubated for
1058 approximately 24 hr until 90-100% confluence. The mouse serum was serially diluted 5-fold in
1059 DMEM, starting at 1:10. The diluted sera were then mixed with titrated virus in a 1:1 (vol/vol)
1060 ratio to generate a mixture containing ~2,000 PFU/well of viruses (MOI = 0.1), followed by an
1061 incubation at 37 °C for 1 hr. Then, the virus/serum mixtures were added to 24-well plates of A549-
1062 ACE2 cells supplemented with 100 µl of DMEM containing 10% FBS in each well. The
1063 supernatant and cell pellet precipitate were then collected, and the viral load was detected by RT-
1064 qPCR. Briefly, RNA was extracted from the cell pellet and reverse transcribed. SARS-CoV-2
1065 RNA quantification was performed by RT-qPCR targeting the N gene of SARS-CoV-2 using a
1066 Roche LightCycler 96. The abundance of *GAPDH* was used as an internal reference. The NT50
1067 was defined as the fold dilution that achieved inhibition of infection exceeding 50% of that of the
1068 control group.

1069

1070 **Mouse challenge experiments**

1071 The mouse model for the SARS-CoV-2 Beta variant challenge has previously been characterized
1072 (Montagutelli et al., 2021). BALB/c mice immunized with circRNA^{RBD-Beta} (50 µg) were
1073 challenged with 5×10^4 PFU SARS-CoV-2 Beta variant at 7 weeks after the boost. The body

1074 weights of the mice were recorded daily. At 3 days after the-challenge, the immunized mice were
1075 sacrificed, and their lung tissues were collected to measure the viral RNA load, as described below.

1076

1077 **Quantification of viral load in mice**

1078 The viral RNA load in the lung tissues of challenged mice was detected by quantitative RT-qPCR.
1079 Briefly, the lung tissues were collected and homogenized with stainless steel beads in TRIZOL (1
1080 ml for each sample). The RNAs in tissues were then extracted and reverse transcribed. SARS-
1081 CoV-2 RNA quantification was performed by RT-qPCR targeting the N gene of SARS-CoV-2
1082 using a Roche LightCycler 96. The abundance of *GAPDH* was used as an internal reference. The
1083 placebo group viral load was normalized to 100%.

1084

1085 **T cell flow cytometry analysis**

1086 The splenocytes from each immunized mouse were cultured in R10 medium (RPMI 1640
1087 supplemented with 1% Pen-Strep antibiotic, 10% HI-FBS) and stimulated with RBD peptide pools
1088 (Table S4) at a final concentration of 2 µg/ml for each peptide. Three hours later, the Golgi Stop
1089 transport inhibitor cocktail (BD) was added according to the manufacturer's instructions. Then, 6
1090 hr later, cells from each group were pooled for stimulation with a cell stimulation cocktail
1091 (PMA/ionomycin) as a positive control. Following stimulation, the cells were washed with PBS
1092 prior to staining with LIVE/DEAD for 20 min at room temperature. Cells were then washed in
1093 stain buffer (PBS supplemented with 2.5% FBS) and suspended in Fc Block for 5 min at RT prior
1094 to staining with a surface stain for the following antibodies: CD3 (Biolegend, #100229); CD4
1095 (Biolegend, #100552); CD8 (Biolegend, #100714); CD44 (Biolegend, #103006); CD62L
1096 (Biolegend, #104445). After 20 min, the cells were washed with staining buffer and then fixed and
1097 permeabilized using a BD Cytoperm fixation/permeabilization solution kit according to the
1098 manufacturer's instructions. Cells were washed in perm/wash solution, followed by intracellular
1099 staining (30 min, RT) using a cocktail of the following antibodies: IFN-γ (Biolegend, #505810);
1100 IL-2 (Biolegend, #503818); IL-4 (Biolegend, #506324); TNF-α (Biolegend, #504104). Finally, the
1101 cells were washed in perm/wash solution and suspended in stain buffer. Samples were washed and
1102 acquired on an LSRFortessa (BD Biosciences). Analysis was performed using FlowJo software.

1103

1104 **Rhesus macaque vaccination and plasma collection**

1105 For the vaccination of rhesus macaques, groups of 2~4-year-old male rhesus macaques were
1106 immunized with LNP-circRNA^{RBD} (20 µg, n = 4; 100 µg, n = 4; 500 µg, n = 4), LNP-circRNA^{Ctrl}
1107 (circRNA without the RBD-encoding sequence; 100 µg, n = 4) or PBS (n = 4) in 300 µl (>300 µl
1108 in 500 µg dose group) via intramuscular injection in the quadriceps muscle (prime: left, boost:
1109 right) twice at a three-week interval. The plasma of immunized rhesus macaques was collected at
1110 0, 1 and 14 days after the prime and 0, 1, 14, 28 and 35 days after post-boost.

1111

1112 **ELISpot assay**

1113 The T cell immune responses in rhesus macaques were detected using PBMCs with commercially
1114 available Monkey IFN-γ and IL-2 ELISpot assay kits (Mabtech) and an Monkey IL-4 ELISpot
1115 assay kit (U-CyTech). The cryopreserved rhesus macaque PBMCs were thawed and cultured with
1116 prewarmed AIM-V medium. For the IFN-γ, IL-2 and IL-4 ELISpot assays, 1.0×10^5 PBMCs were
1117 stimulated with a final concentration of 1 µg/ml for each RBD peptide (Table S5). The test for
1118 each rhesus macaque was performed in two or three technical repetitions. Dimethyl sulfoxide
1119 (DMSO) served as an unstimulating control, and phytohemagglutinin (PHA-P, Sigma) and CELL
1120 STIMULATION COCKTAIL (Thermo Fisher) were used as positive controls. After 24 h of
1121 stimulation with RBD peptide pools, the streptavidin-HRP substrate (for IFN-γ and IL-2) or AEC
1122 substrate (IL-4) was added to the plate. The spots were counted by Beijing Dakewei Biotechnology
1123 Co., Ltd. The results are background (DMSO treated group) subtracted and normalized to SFC/ 10^6
1124 PBMCs.

1125

1126 **SARS-CoV-2 challenge in rhesus macaques**

1127 At 5 weeks after the boost, all the immunized rhesus macaques were challenged with 1.0×10^6 PFU
1128 of native SARS-CoV-2 virus via the intranasal (0.5 ml) and intratracheal (0.5 ml) routes. The
1129 plasma of rhesus macaques was collected, and vital clinical signs were recorded at 0, 1, 3, 5 and 7
1130 days post-virus challenge. At 7 days post-virus challenge, all rhesus macaques were sacrificed to
1131 collect specimens for further experiments.

1132

1133 **Histopathology**

1134 At 7 days after the-virus challenge, the rhesus monkeys were euthanized, and necropsies were
1135 performed according to standard protocols. After dissection, a general examination of the main

1136 organs was performed. The lung tissues were harvested, fixed in 10% neutral formalin buffer and
1137 embedded in paraffin. Tissue sections (2 μ m) were prepared. Slides were stained with hematoxylin
1138 and eosin (H&E). The slide images were collected by using Panoramic DESK and analyzed with
1139 Caseviewer C. V 2.3 and Image-Pro Plus 6.0. Histopathological analysis of tissue slides was scored
1140 by 3 independent pathologists blinded to the groups of animals.

1141

1142 **Cytokine analysis**

1143 The plasma of rhesus monkeys was isolated 24 hr post-prime or boost and diluted 5-fold or 10-
1144 fold. All plasma samples were detected using the following ELISA kits according to the
1145 manufacturer's instructions: IL-6 (Abcam, #ab242233), MCP-1 (Cloud-Clone Corp.,
1146 #SEA087Si96T), TNF- α (Abcam, #ab252354), IL-1 β (Cloud-clone Corp, #SEA563Si96T) and
1147 IFN- α (Chenglin, #AD0081Mk), according to the manufacturer's instructions.

1148

1149 **QUANTIFICATION AND STATISTICAL ANALYSIS**

1150 The unpaired two-sided Student's *t* test or paired Student's *t* test was performed for comparison as
1151 indicated in the figure legends. Statistical analyses were performed with Prism 8 (GraphPad
1152 Software, Inc.).

1153

1154

1155 **SUPPLEMENTAL INFORMATION**

1156

1157 Table S1. The sequences of the circRNA^{RBD} produced via group I intron, Related to Figures 1-6

1158

1159 Table S2. The sequences of the circRNA^{RBD} produced via T4 RNA ligases, Related to Figures 1
1160 and 2

1161

1162 Table S3. The sequences of the mRNA^{RBD-Delta}, Related to Figures 3-5

1163

1164 Table S4. The peptide sequences of the RBD-Delta antigen, Related to Figure 4

1165

1166 Table S5. The peptide sequences of the RBD antigen, Related to Figures 4 and 6

1167

1168

1169

1170 **REFERENCES**

- 1171 Alameh, M.G., Tombacz, I., Bettini, E., Lederer, K., Sittplangkoon, C., Wilmore, J.R., Gaudette, B.T., Soliman,
1172 O.Y., Pine, M., Hicks, P., *et al.* (2021). Lipid nanoparticles enhance the efficacy of mRNA and protein subunit
1173 vaccines by inducing robust T follicular helper cell and humoral responses. *Immunity* 54, 2877-2892 e2877.
- 1174 Bangaru, S., Ozorowski, G., Turner, H.L., Antanasijevic, A., Huang, D., Wang, X., Torres, J.L., Diedrich, J.K.,
1175 Tian, J.H., Portnoff, A.D., *et al.* (2020). Structural analysis of full-length SARS-CoV-2 spike protein from an
1176 advanced vaccine candidate. *Science* 370, 1089-1094.
- 1177 Barnes, C.O., Jette, C.A., Abernathy, M.E., Dam, K.A., Esswein, S.R., Gristick, H.B., Malyutin, A.G., Sharaf, N.G.,
1178 Huey-Tubman, K.E., Lee, Y.E., *et al.* (2020). SARS-CoV-2 neutralizing antibody structures inform therapeutic
1179 strategies. *Nature* 588, 682-687.
- 1180 Boutros, C., Tarhini, A., Routier, E., Lambotte, O., Ladurie, F.L., Carbonnel, F., Izzeddine, H., Marabelle, A.,
1181 Champiat, S., Berdelou, A., *et al.* (2016). Safety profiles of anti-CTLA-4 and anti-PD-1 antibodies alone and in
1182 combination. *Nat Rev Clin Oncol* 13, 473-486.
- 1183 Bouwman, K.M., Tomris, I., Turner, H.L., van der Woude, R., Shamorkina, T.M., Bosman, G.P., Rockx, B., Herfst,
1184 S., Snijder, J., Haagmans, B.L., *et al.* (2021). Multimerization- and glycosylation-dependent receptor binding of
1185 SARS-CoV-2 spike proteins. *PLoS Pathog* 17, e1009282.
- 1186 Cameroni, E., Bowen, J.E., Rosen, L.E., Saliba, C., Zepeda, S.K., Culap, K., Pinto, D., VanBlargan, L.A., De
1187 Marco, A., di Iulio, J., *et al.* (2021). Broadly neutralizing antibodies overcome SARS-CoV-2 Omicron antigenic
1188 shift. *Nature*.
- 1189 Cao, Y., Su, B., Guo, X., Sun, W., Deng, Y., Bao, L., Zhu, Q., Zhang, X., Zheng, Y., Geng, C., *et al.* (2020). Potent
1190 Neutralizing Antibodies against SARS-CoV-2 Identified by High-Throughput Single-Cell Sequencing of
1191 Convalescent Patients' B Cells. *Cell* 182, 73-84 e16.
- 1192 Cao, Y., Wang, J., Jian, F., Xiao, T., Song, W., Yisimayi, A., Huang, W., Li, Q., Wang, P., An, R., *et al.* (2021).
1193 Omicron escapes the majority of existing SARS-CoV-2 neutralizing antibodies. *Nature*.
- 1194 Cele, S., Jackson, L., Khoury, D.S., Khan, K., Moyo-Gwete, T., Tegally, H., San, J.E., Cromer, D., Scheepers, C.,
1195 Amoako, D., *et al.* (2021). Omicron extensively but incompletely escapes Pfizer BNT162b2 neutralization. *Nature*.
- 1196 Chan, K.K., Dorosky, D., Sharma, P., Abbasi, S.A., Dye, J.M., Kranz, D.M., Herbert, A.S., and Procko, E. (2020).
1197 Engineering human ACE2 to optimize binding to the spike protein of SARS coronavirus 2. *Science* 369, 1261-1265.
- 1198 Chen, L.L. (2016). The biogenesis and emerging roles of circular RNAs. *Nat Rev Mol Cell Biol* 17, 205-211.
- 1199 Chen, Q., Huang, X.Y., Sun, M.X., Li, R.T., Gu, H., Tian, Y., Zhang, R.R., Luo, D., Zhou, C., Zhang, Y., *et al.*
1200 (2021). Transient acquisition of cross-species infectivity during the evolution of SARS-CoV-2. *Natl Sci Rev* 8,
1201 nwab167.
- 1202 Chen, Y.G., Chen, R., Ahmad, S., Verma, R., Kasturi, S.P., Amaya, L., Broughton, J.P., Kim, J., Cadena, C.,
1203 Pulendran, B., *et al.* (2019). N6-Methyladenosine Modification Controls Circular RNA Immunity. *Mol Cell* 76, 96-
1204 109 e109.

- 1205 Corbett, K.S., Edwards, D.K., Leist, S.R., Abiona, O.M., Boyoglu-Barnum, S., Gillespie, R.A., Himansu, S.,
1206 Schafer, A., Ziwawo, C.T., DiPiazza, A.T., *et al.* (2020a). SARS-CoV-2 mRNA vaccine design enabled by
1207 prototype pathogen preparedness. *Nature* 586, 567-571.
- 1208 Corbett, K.S., Flynn, B., Foulds, K.E., Francica, J.R., Boyoglu-Barnum, S., Werner, A.P., Flach, B., O'Connell, S.,
1209 Bock, K.W., Minai, M., *et al.* (2020b). Evaluation of the mRNA-1273 Vaccine against SARS-CoV-2 in Nonhuman
1210 Primates. *N Engl J Med* 383, 1544-1555.
- 1211 Dai, L., Zheng, T., Xu, K., Han, Y., Xu, L., Huang, E., An, Y., Cheng, Y., Li, S., Liu, M., *et al.* (2020). A Universal
1212 Design of Betacoronavirus Vaccines against COVID-19, MERS, and SARS. *Cell* 182, 722-733 e711.
- 1213 Dejnirattisai, W., Huo, J., Zhou, D., Zahradník, J., Supasa, P., Liu, C., Duyvesteyn, H.M.E., Ginn, H.M., Mentzer,
1214 A.J., Tuekprakhon, A., *et al.* (2022). SARS-CoV-2 Omicron-B.1.1.529 leads to widespread escape from neutralizing
1215 antibody responses. *Cell*.
- 1216 Dejnirattisai, W., Jumnainsong, A., Onsirisakul, N., Fitton, P., Vasanawathana, S., Limpitikul, W., Puttikhunt, C.,
1217 Edwards, C., Duangchinda, T., Supasa, S., *et al.* (2010). Cross-reacting antibodies enhance dengue virus infection in
1218 humans. *Science* 328, 745-748.
- 1219 Dowd, K.A., and Pierson, T.C. (2011). Antibody-mediated neutralization of flaviviruses: a reductionist view.
1220 *Virology* 411, 306-315.
- 1221 Du, S., Cao, Y., Zhu, Q., Yu, P., Qi, F., Wang, G., Du, X., Bao, L., Deng, W., Zhu, H., *et al.* (2020). Structurally
1222 Resolved SARS-CoV-2 Antibody Shows High Efficacy in Severely Infected Hamsters and Provides a Potent
1223 Cocktail Pairing Strategy. *Cell* 183, 1013-1023 e1013.
- 1224 Durymanov, M., and Reineke, J. (2018). Non-viral Delivery of Nucleic Acids: Insight Into Mechanisms of
1225 Overcoming Intracellular Barriers. *Front Pharmacol* 9, 971.
- 1226 Enuka, Y., Lauriola, M., Feldman, M.E., Sas-Chen, A., Ulitsky, I., and Yarden, Y. (2016). Circular RNAs are long-
1227 lived and display only minimal early alterations in response to a growth factor. *Nucleic Acids Res* 44, 1370-1383.
- 1228 Fenton, O.S., Kauffman, K.J., McClellan, R.L., Appel, E.A., Dorkin, J.R., Tibbitt, M.W., Heartlein, M.W., DeRosa,
1229 F., Langer, R., and Anderson, D.G. (2016). Bioinspired Alkenyl Amino Alcohol Ionizable Lipid Materials for
1230 Highly Potent In Vivo mRNA Delivery. *Adv Mater* 28, 2939-2943.
- 1231 Fischer, J.W., and Leung, A.K. (2017). CircRNAs: a regulator of cellular stress. *Crit Rev Biochem Mol Biol* 52,
1232 220-233.
- 1233 Gao, Q., Bao, L., Mao, H., Wang, L., Xu, K., Yang, M., Li, Y., Zhu, L., Wang, N., Lv, Z., *et al.* (2020).
1234 Development of an inactivated vaccine candidate for SARS-CoV-2. *Science* 369, 77-81.
- 1235 Gao, X., Xia, X., Li, F., Zhang, M., Zhou, H., Wu, X., Zhong, J., Zhao, Z., Zhao, K., Liu, D., *et al.* (2021). Circular
1236 RNA-encoded oncogenic E-cadherin variant promotes glioblastoma tumorigenicity through activation of EGFR-
1237 STAT3 signalling. *Nat Cell Biol*.
- 1238 Garcia-Beltran, W.F., St Denis, K.J., Hoelzemer, A., Lam, E.C., Nitido, A.D., Sheehan, M.L., Berrios, C., Ofoman,
1239 O., Chang, C.C., Hauser, B.M., *et al.* (2022). mRNA-based COVID-19 vaccine boosters induce neutralizing
1240 immunity against SARS-CoV-2 Omicron variant. *Cell* 185, 457-466 e454.

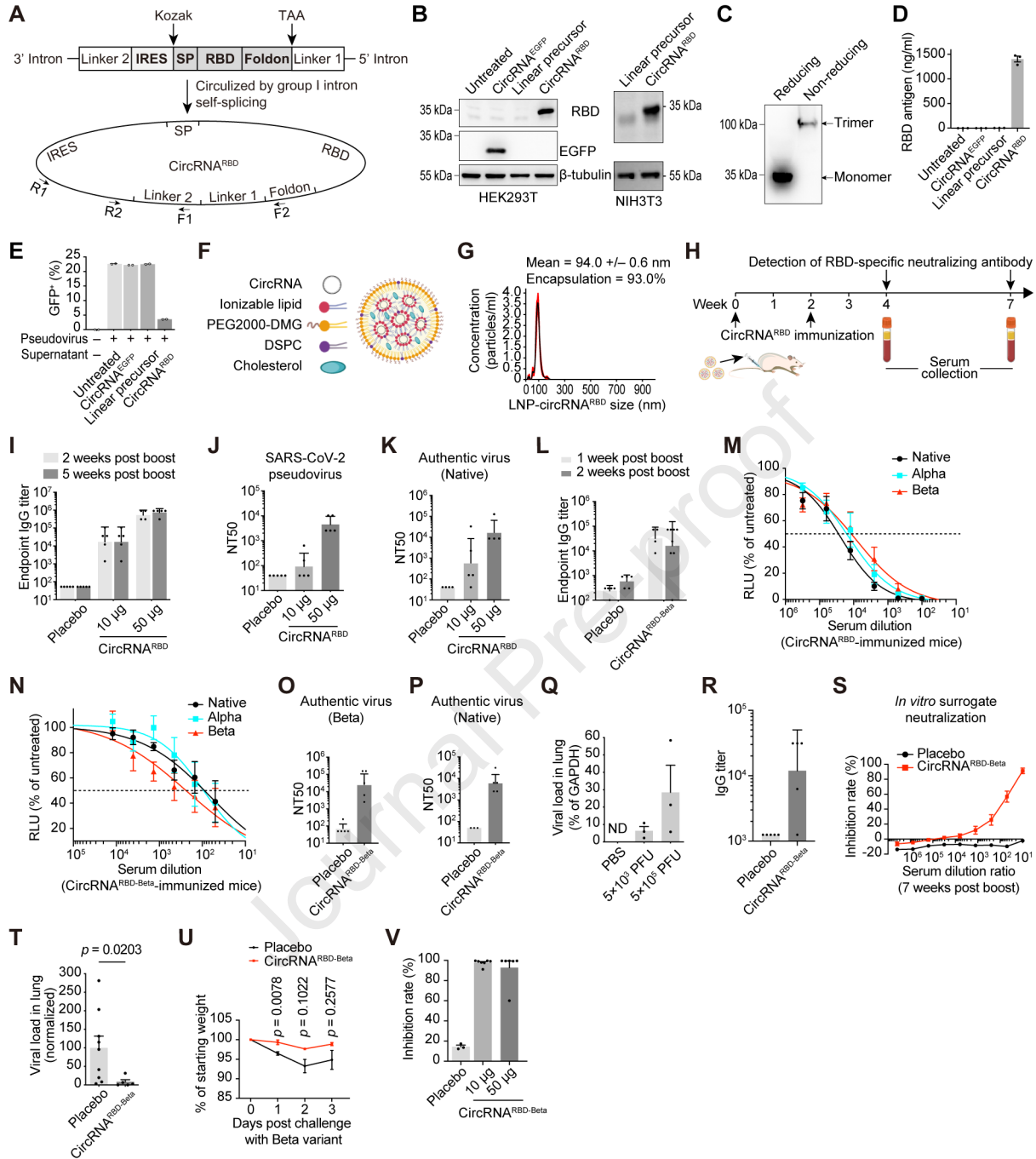
- 1241 Glasgow, A., Glasgow, J., Limonta, D., Solomon, P., Lui, I., Zhang, Y., Nix, M.A., Rettko, N.J., Zha, S., Yamin, R.,
1242 *et al.* (2020). Engineered ACE2 receptor traps potently neutralize SARS-CoV-2. *Proc Natl Acad Sci U S A* *117*,
1243 28046-28055.
- 1244 Graham, B.S. (2020). Rapid COVID-19 vaccine development. *Science* *368*, 945-946.
- 1245 Gu, H., Chen, Q., Yang, G., He, L., Fan, H., Deng, Y.Q., Wang, Y., Teng, Y., Zhao, Z., Cui, Y., *et al.* (2020).
1246 Adaptation of SARS-CoV-2 in BALB/c mice for testing vaccine efficacy. *Science* *369*, 1603-1607.
- 1247 Halstead, S.B., and O'Rourke, E.J. (1977). Dengue viruses and mononuclear phagocytes. I. Infection enhancement
1248 by non-neutralizing antibody. *J Exp Med* *146*, 201-217.
- 1249 He, X., and Xu, C. (2020). Immune checkpoint signaling and cancer immunotherapy. *Cell Res* *30*, 660-669.
- 1250 Hoffmann, M., Kleine-Weber, H., Schroeder, S., Kruger, N., Herrler, T., Erichsen, S., Schiergens, T.S., Herrler, G.,
1251 Wu, N.H., Nitsche, A., *et al.* (2020). SARS-CoV-2 Cell Entry Depends on ACE2 and TMPRSS2 and Is Blocked by
1252 a Clinically Proven Protease Inhibitor. *Cell* *181*, 271-280 e278.
- 1253 Hsieh, C.L., Goldsmith, J.A., Schaub, J.M., DiVenere, A.M., Kuo, H.C., Javanmardi, K., Le, K.C., Wrapp, D., Lee,
1254 A.G., Liu, Y., *et al.* (2020). Structure-based design of prefusion-stabilized SARS-CoV-2 spikes. *Science* *369*, 1501-
1255 1505.
- 1256 Huang, Q., Ji, K., Tian, S., Wang, F., Huang, B., Tong, Z., Tan, S., Hao, J., Wang, Q., Tan, W., *et al.* (2021). A
1257 single-dose mRNA vaccine provides a long-term protection for hACE2 transgenic mice from SARS-CoV-2. *Nature*
1258 *communications* *12*, 776.
- 1259 Ickenstein, L.M., and Garidel, P. (2019). Lipid-based nanoparticle formulations for small molecules and RNA drugs.
1260 *Expert Opin Drug Deliv* *16*, 1205-1226.
- 1261 Jackson, N.A.C., Kester, K.E., Casimiro, D., Gurunathan, S., and DeRosa, F. (2020). The promise of mRNA
1262 vaccines: a biotech and industrial perspective. *NPJ Vaccines* *5*, 11.
- 1263 Kariko, K., Buckstein, M., Ni, H., and Weissman, D. (2005). Suppression of RNA recognition by Toll-like
1264 receptors: the impact of nucleoside modification and the evolutionary origin of RNA. *Immunity* *23*, 165-175.
- 1265 Karim, S.S.A., and Karim, Q.A. (2021). Omicron SARS-CoV-2 variant: a new chapter in the COVID-19 pandemic.
1266 *Lancet* *398*, 2126-2128.
- 1267 Khan, K., Karim, F., Cele, S., San, J.E., Lustig, G., Tegally, H., Bernstein, M., Ganga, Y., Jule, Z., Reedoy, K., *et al.*
1268 (2021). Omicron infection enhances neutralizing immunity against the Delta variant. *medRxiv*.
- 1269 Kim, D., Lee, J.Y., Yang, J.S., Kim, J.W., Kim, V.N., and Chang, H. (2020). The Architecture of SARS-CoV-2
1270 Transcriptome. *Cell* *181*, 914-921 e910.
- 1271 Koenig, P.A., Das, H., Liu, H., Kummerer, B.M., Gohr, F.N., Jenster, L.M., Schifferers, L.D.J., Tesfamariam, Y.M.,
1272 Uchima, M., Wuerth, J.D., *et al.* (2021). Structure-guided multivalent nanobodies block SARS-CoV-2 infection and
1273 suppress mutational escape. *Science* *371*.
- 1274 Kou, Y., Xu, Y., Zhao, Z., Liu, J., Wu, Y., You, Q., Wang, L., Gao, F., Cai, L., and Jiang, C. (2017). Tissue
1275 plasminogen activator (tPA) signal sequence enhances immunogenicity of MVA-based vaccine against tuberculosis.
1276 *Immunol Lett* *190*, 51-57.
- 1277 Krammer, F. (2020). SARS-CoV-2 vaccines in development. *Nature* *586*, 516-527.

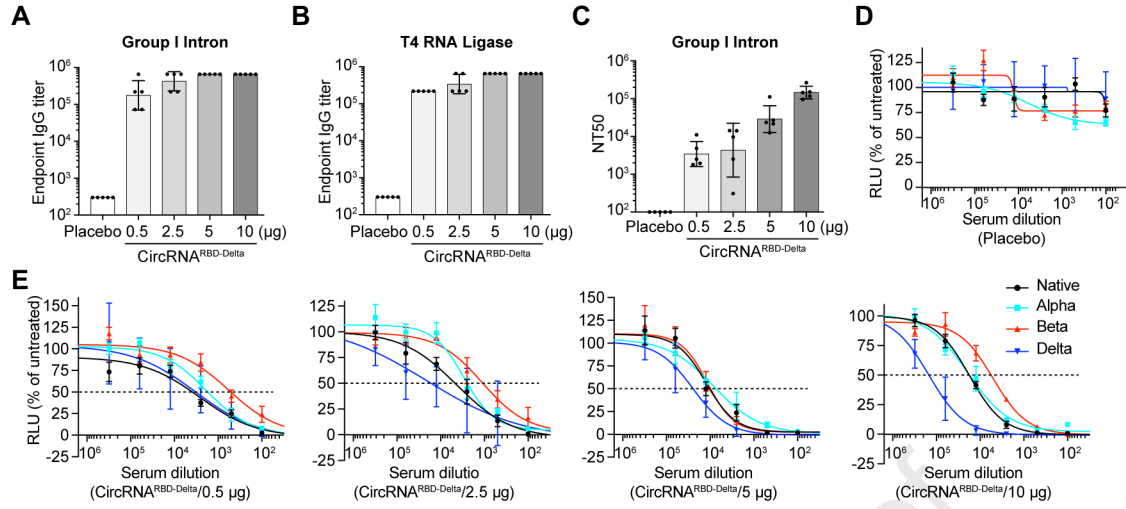
- 1278 Kristensen, L.S., Andersen, M.S., Stagsted, L.V.W., Ebbesen, K.K., Hansen, T.B., and Kjems, J. (2019). The
1279 biogenesis, biology and characterization of circular RNAs. *Nat Rev Genet* 20, 675-691.
- 1280 Laczko, D., Hogan, M.J., Toulmin, S.A., Hicks, P., Lederer, K., Gaudette, B.T., Castano, D., Amanat, F.,
1281 Muramatsu, H., Oguin, T.H., 3rd, *et al.* (2020). A Single Immunization with Nucleoside-Modified mRNA Vaccines
1282 Elicits Strong Cellular and Humoral Immune Responses against SARS-CoV-2 in Mice. *Immunity* 53, 724-732 e727.
- 1283 Legnini, I., Di Timoteo, G., Rossi, F., Morlando, M., Briganti, F., Sthandier, O., Fatica, A., Santini, T., Andronache,
1284 A., Wade, M., *et al.* (2017). Circ-ZNF609 Is a Circular RNA that Can Be Translated and Functions in Myogenesis.
1285 *Mol Cell* 66, 22-37 e29.
- 1286 Linsky, T.W., Vergara, R., Codina, N., Nelson, J.W., Walker, M.J., Su, W., Barnes, C.O., Hsiang, T.Y., Esser-
1287 Nobis, K., Yu, K., *et al.* (2020). De novo design of potent and resilient hACE2 decoys to neutralize SARS-CoV-2.
1288 *Science* 370, 1208-1214.
- 1289 Liu, B., Lin, Y., Yan, J., Yao, J., Liu, D., Ma, W., Wang, J., Liu, W., Wang, C., Zhang, L., *et al.* (2021a). Affinity-
1290 coupled CCL22 promotes positive selection in germinal centres. *Nature* 592, 133-137.
- 1291 Liu, C.X., Guo, S.K., Nan, F., Xu, Y.F., Yang, L., and Chen, L.L. (2021b). RNA circles with minimized
1292 immunogenicity as potent PKR inhibitors. *Mol Cell*.
- 1293 Liu, L., Iketani, S., Guo, Y., Chan, J.F.W., Wang, M., Liu, L., Luo, Y., Chu, H., Huang, Y., Nair, M.S., *et al.*
1294 (2021c). Striking antibody evasion manifested by the Omicron variant of SARS-CoV-2. *Nature*.
- 1295 Lustig, Y., Zuckerman, N., Nemet, I., Atari, N., Kliker, L., Regev-Yochay, G., Sapir, E., Mor, O., Alroy-Preis, S.,
1296 Mendelson, E., *et al.* (2021). Neutralising capacity against Delta (B.1.617.2) and other variants of concern following
1297 Comirnaty (BNT162b2, BioNTech/Pfizer) vaccination in health care workers, Israel. *Euro Surveill* 26.
- 1298 Martinez-Vega, R.A., Carrasquilla, G., Luna, E., and Ramos-Castaneda, J. (2017). ADE and dengue vaccination.
1299 *Vaccine* 35, 3910-3912.
- 1300 Memczak, S., Jens, M., Elefsinioti, A., Torti, F., Krueger, J., Rybak, A., Maier, L., Mackowiak, S.D., Gregersen,
1301 L.H., Munschauer, M., *et al.* (2013). Circular RNAs are a large class of animal RNAs with regulatory potency.
1302 *Nature* 495, 333-338.
- 1303 Montagutelli, X., Prot, M., Levillayer, L., Salazar, E.B., Jouvion, G., Conquet, L., Donati, F., Albert, M., Gambaro,
1304 F., Behillil, S., *et al.* (2021). Variants with the N501Y mutation extend SARS-CoV-2 host range to mice, with
1305 contact transmission. *bioRxiv*.
- 1306 Muik, A., Wallisch, A.K., Sanger, B., Swanson, K.A., Muhl, J., Chen, W., Cai, H., Maurus, D., Sarkar, R., Tureci,
1307 O., *et al.* (2021). Neutralization of SARS-CoV-2 lineage B.1.1.7 pseudovirus by BNT162b2 vaccine-elicited human
1308 sera. *Science*.
- 1309 Mukhopadhyay, S., Vander Heiden, M.G., and McCormick, F. (2021). The Metabolic Landscape of RAS-Driven
1310 Cancers from biology to therapy. *Nat Cancer* 2, 271-283.
- 1311 Mullard, A. (2020). COVID-19 vaccine development pipeline gears up. *Lancet* 395, 1751-1752.
- 1312 Ou, X., Liu, Y., Lei, X., Li, P., Mi, D., Ren, L., Guo, L., Guo, R., Chen, T., Hu, J., *et al.* (2020). Characterization of
1313 spike glycoprotein of SARS-CoV-2 on virus entry and its immune cross-reactivity with SARS-CoV. *Nat Commun*
1314 11, 1620.

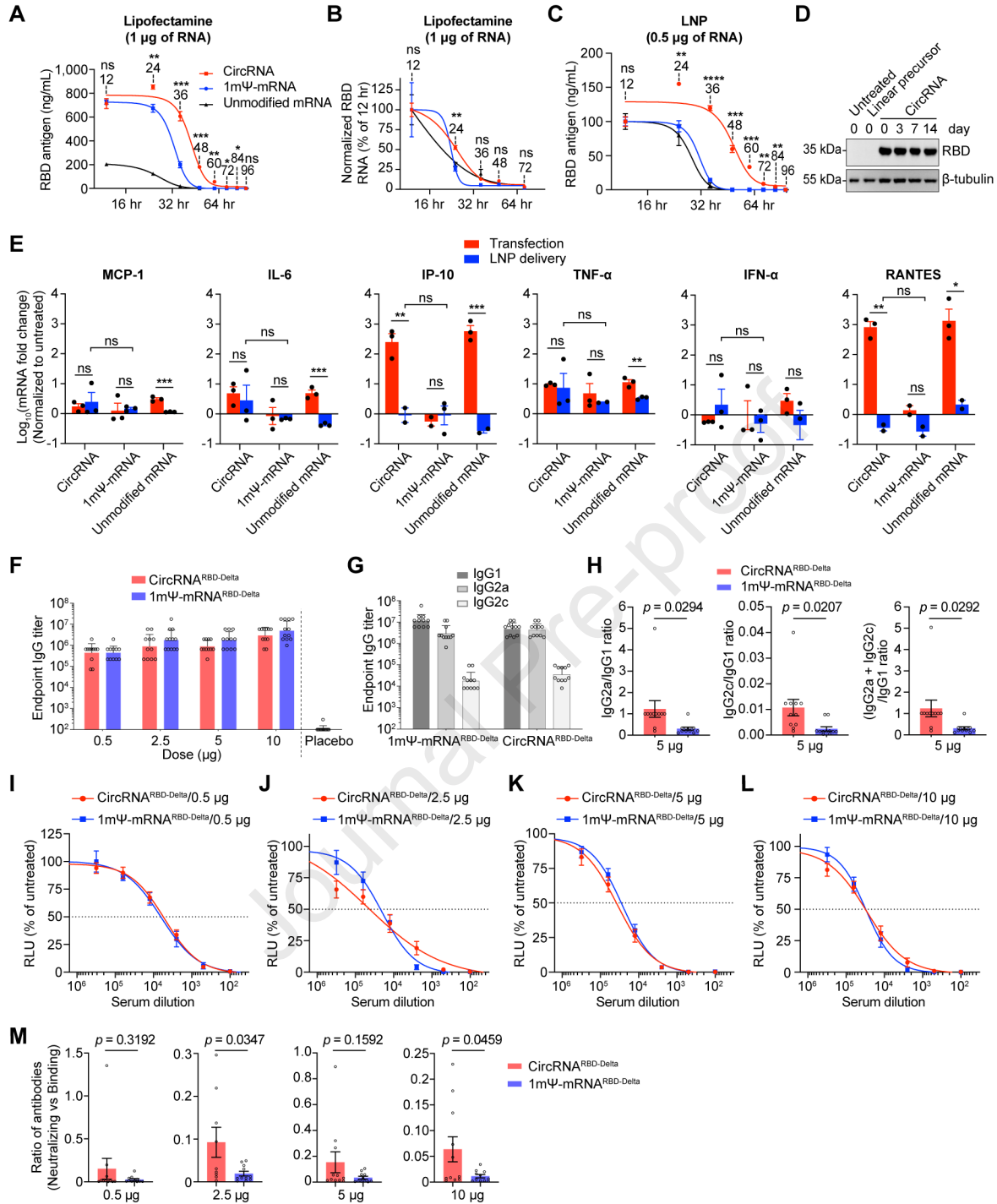
- 1315 Papanikolopoulou, K., van Raaij, M.J., and Mitraki, A. (2008). Creation of hybrid nanorods from sequences of
1316 natural trimeric fibrous proteins using the fibrinin trimerization motif. *Methods Mol Biol* 474, 15-33.
- 1317 Pardi, N., Hogan, M.J., Pelc, R.S., Muramatsu, H., Andersen, H., DeMaso, C.R., Dowd, K.A., Sutherland, L.L.,
1318 Scarce, R.M., Parks, R., *et al.* (2017). Zika virus protection by a single low-dose nucleoside-modified mRNA
1319 vaccination. *Nature* 543, 248-251.
- 1320 Pardi, N., Hogan, M.J., Porter, F.W., and Weissman, D. (2018). mRNA vaccines - a new era in vaccinology. *Nat*
1321 *Rev Drug Discov* 17, 261-279.
- 1322 Planas, D., Saunders, N., Maes, P., Guivel-Benhassine, F., Planchais, C., Buchrieser, J., Bolland, W.-H., Porrot, F.,
1323 Staropoli, I., Lemoine, F., *et al.* (2021a). Considerable escape of SARS-CoV-2 Omicron to antibody neutralization.
1324 *Nature*.
- 1325 Planas, D., Veyer, D., Baidaliuk, A., Staropoli, I., Guivel-Benhassine, F., Rajah, M.M., Planchais, C., Porrot, F.,
1326 Robillard, N., Puech, J., *et al.* (2021b). Reduced sensitivity of SARS-CoV-2 variant Delta to antibody neutralization.
1327 *Nature* 596, 276-280.
- 1328 Rey, F.A., Stiasny, K., Vaney, M.C., Dellarole, M., and Heinz, F.X. (2018). The bright and the dark side of human
1329 antibody responses to flaviviruses: lessons for vaccine design. *EMBO Rep* 19, 206-224.
- 1330 Richner, J.M., Himansu, S., Dowd, K.A., Butler, S.L., Salazar, V., Fox, J.M., Julander, J.G., Tang, W.W., Shresta,
1331 S., Pierson, T.C., *et al.* (2017). Modified mRNA Vaccines Protect against Zika Virus Infection. *Cell* 169, 176.
- 1332 Routhu, N.K., Cheedarla, N., Bollimpelli, V.S., Gangadhara, S., Edara, V.V., Lai, L., Sahoo, A., Shiferaw, A.,
1333 Styles, T.M., Floyd, K., *et al.* (2021). SARS-CoV-2 RBD trimer protein adjuvanted with Alum-3M-052 protects
1334 from SARS-CoV-2 infection and immune pathology in the lung. *Nat Commun* 12, 3587.
- 1335 Sabapathy, K., and Lane, D.P. (2018). Therapeutic targeting of p53: all mutants are equal, but some mutants are
1336 more equal than others. *Nat Rev Clin Oncol* 15, 13-30.
- 1337 Sahin, U., Muik, A., Derhovanessian, E., Vogler, I., Kranz, L.M., Vormehr, M., Baum, A., Pascal, K., Quandt, J.,
1338 Maurus, D., *et al.* (2020). COVID-19 vaccine BNT162b1 elicits human antibody and TH1 T cell responses. *Nature*
1339 586, 594-599.
- 1340 Sanchez-Felipe, L., Vercruyse, T., Sharma, S., Ma, J., Lemmens, V., Van Looveren, D., Arkalagud Javarappa,
1341 M.P., Boudewijns, R., Malengier-Devlies, B., Liesenborghs, L., *et al.* (2021). A single-dose live-attenuated YF17D-
1342 vectored SARS-CoV-2 vaccine candidate. *Nature* 590, 320-325.
- 1343 Schoof, M., Faust, B., Saunders, R.A., Sangwan, S., Rezelj, V., Hoppe, N., Boone, M., Billesbolle, C.B., Puchades,
1344 C., Azumaya, C.M., *et al.* (2020). An ultrapotent synthetic nanobody neutralizes SARS-CoV-2 by stabilizing
1345 inactive Spike. *Science* 370, 1473-1479.
- 1346 Sette, A., and Crotty, S. (2021). Adaptive immunity to SARS-CoV-2 and COVID-19. *Cell* 184, 861-880.
- 1347 Shang, J., Wan, Y., Luo, C., Ye, G., Geng, Q., Auerbach, A., and Li, F. (2020). Cell entry mechanisms of SARS-
1348 CoV-2. *Proc Natl Acad Sci U S A* 117, 11727-11734.
- 1349 Tai, W., Zhang, X., Drelich, A., Shi, J., Hsu, J.C., Luchsinger, L., Hillyer, C.D., Tseng, C.K., Jiang, S., and Du, L.
1350 (2020). A novel receptor-binding domain (RBD)-based mRNA vaccine against SARS-CoV-2. *Cell Res* 30, 932-935.

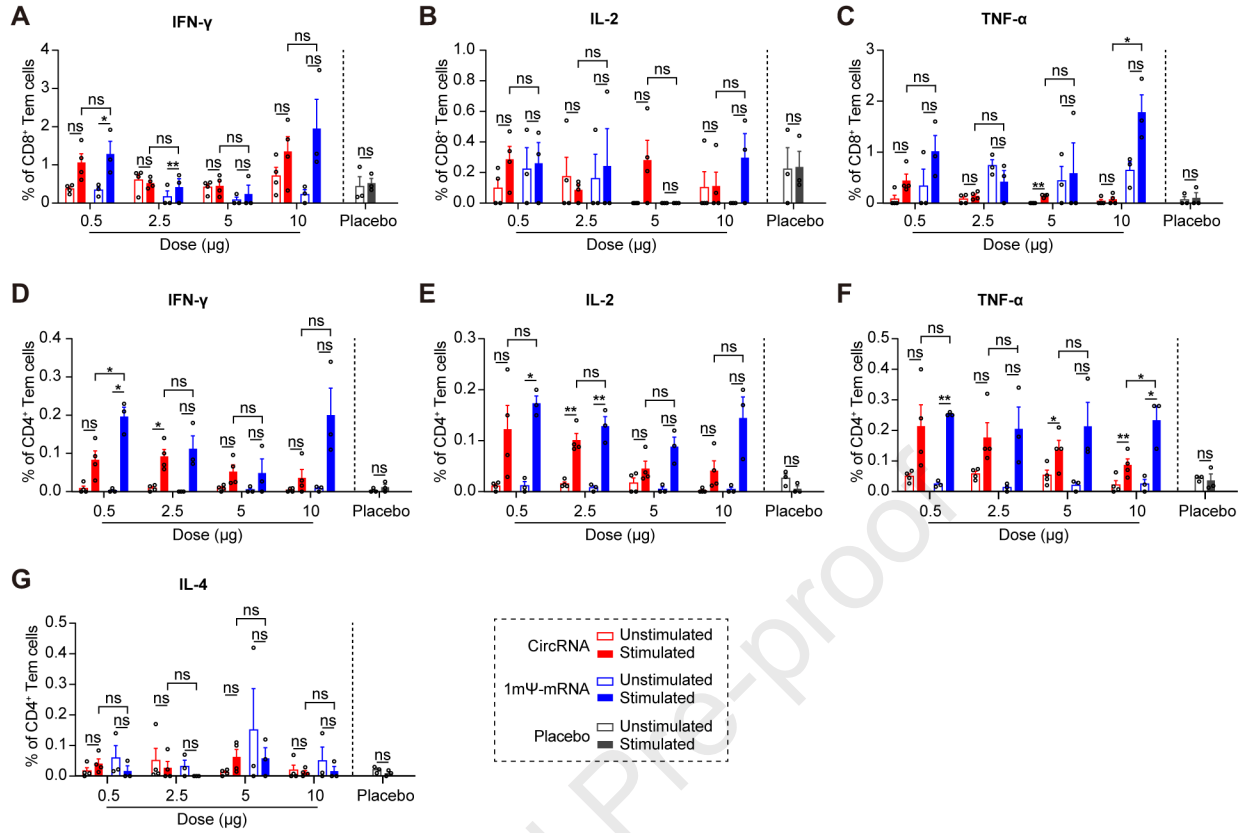
- 1351 Takano, T., Yamada, S., Doki, T., and Hohdatsu, T. (2019). Pathogenesis of oral type I feline infectious peritonitis
1352 virus (FIPV) infection: Antibody-dependent enhancement infection of cats with type I FIPV via the oral route. *J Vet*
1353 *Med Sci* *81*, 911-915.
- 1354 Torgovnick, J. (2021). Effectiveness of Covid-19 Vaccines against the B.1.617.2 (Delta) Variant. *N Engl J Med* *385*,
1355 e92.
- 1356 Uddin, M.N., and Roni, M.A. (2021). Challenges of Storage and Stability of mRNA-Based COVID-19 Vaccines.
1357 *Vaccines (Basel)* *9*.
- 1358 V'Kovski, P., Kratzel, A., Steiner, S., Stalder, H., and Thiel, V. (2021). Coronavirus biology and replication:
1359 implications for SARS-CoV-2. *Nat Rev Microbiol* *19*, 155-170.
- 1360 van Doremalen, N., Lambe, T., Spencer, A., Belij-Rammerstorfer, S., Purushotham, J.N., Port, J.R., Avanzato, V.A.,
1361 Bushmaker, T., Flaxman, A., Ulaszewska, M., *et al.* (2020). ChAdOx1 nCoV-19 vaccine prevents SARS-CoV-2
1362 pneumonia in rhesus macaques. *Nature* *586*, 578-582.
- 1363 Vogel, A.B., Kanevsky, I., Che, Y., Swanson, K.A., Muik, A., Vormehr, M., Kranz, L.M., Walzer, K.C., Hein, S.,
1364 Guler, A., *et al.* (2021). BNT162b vaccines protect rhesus macaques from SARS-CoV-2. *Nature*.
- 1365 Walls, A.C., Park, Y.J., Tortorici, M.A., Wall, A., McGuire, A.T., and Veessler, D. (2020). Structure, Function, and
1366 Antigenicity of the SARS-CoV-2 Spike Glycoprotein. *Cell* *181*, 281-292 e286.
- 1367 Wang, P., Nair, M.S., Liu, L., Iketani, S., Luo, Y., Guo, Y., Wang, M., Yu, J., Zhang, B., Kwong, P.D., *et al.*
1368 (2021a). Antibody Resistance of SARS-CoV-2 Variants B.1.351 and B.1.1.7. *Nature*.
- 1369 Wang, Z., Schmidt, F., Weisblum, Y., Muecksch, F., Barnes, C.O., Finkin, S., Schaefer-Babajew, D., Cipolla, M.,
1370 Gaebler, C., Lieberman, J.A., *et al.* (2021b). mRNA vaccine-elicited antibodies to SARS-CoV-2 and circulating
1371 variants. *Nature*.
- 1372 Wen, J., Cheng, Y., Ling, R., Dai, Y., Huang, B., Huang, W., Zhang, S., and Jiang, Y. (2020). Antibody-dependent
1373 enhancement of coronavirus. *Int J Infect Dis* *100*, 483-489.
- 1374 Wesselhoef, R.A., Kowalski, P.S., and Anderson, D.G. (2018). Engineering circular RNA for potent and stable
1375 translation in eukaryotic cells. *Nat Commun* *9*, 2629.
- 1376 Wesselhoef, R.A., Kowalski, P.S., Parker-Hale, F.C., Huang, Y., Bisaria, N., and Anderson, D.G. (2019). RNA
1377 Circularization Diminishes Immunogenicity and Can Extend Translation Duration In Vivo. *Mol Cell* *74*, 508-520
1378 e504.
- 1379 Wrapp, D., Wang, N., Corbett, K.S., Goldsmith, J.A., Hsieh, C.L., Abiona, O., Graham, B.S., and McLellan, J.S.
1380 (2020). Cryo-EM structure of the 2019-nCoV spike in the prefusion conformation. *Science* *367*, 1260-1263.
- 1381 Wu, F., Zhao, S., Yu, B., Chen, Y.M., Wang, W., Song, Z.G., Hu, Y., Tao, Z.W., Tian, J.H., Pei, Y.Y., *et al.* (2020).
1382 A new coronavirus associated with human respiratory disease in China. *Nature* *579*, 265-269.
- 1383 Xiang, Y., Nambulli, S., Xiao, Z., Liu, H., Sang, Z., Duprex, W.P., Schneidman-Duhovny, D., Zhang, C., and Shi,
1384 Y. (2020). Versatile and multivalent nanobodies efficiently neutralize SARS-CoV-2. *Science* *370*, 1479-1484.
- 1385 Yan, R., Zhang, Y., Li, Y., Xia, L., Guo, Y., and Zhou, Q. (2020). Structural basis for the recognition of SARS-
1386 CoV-2 by full-length human ACE2. *Science* *367*, 1444-1448.

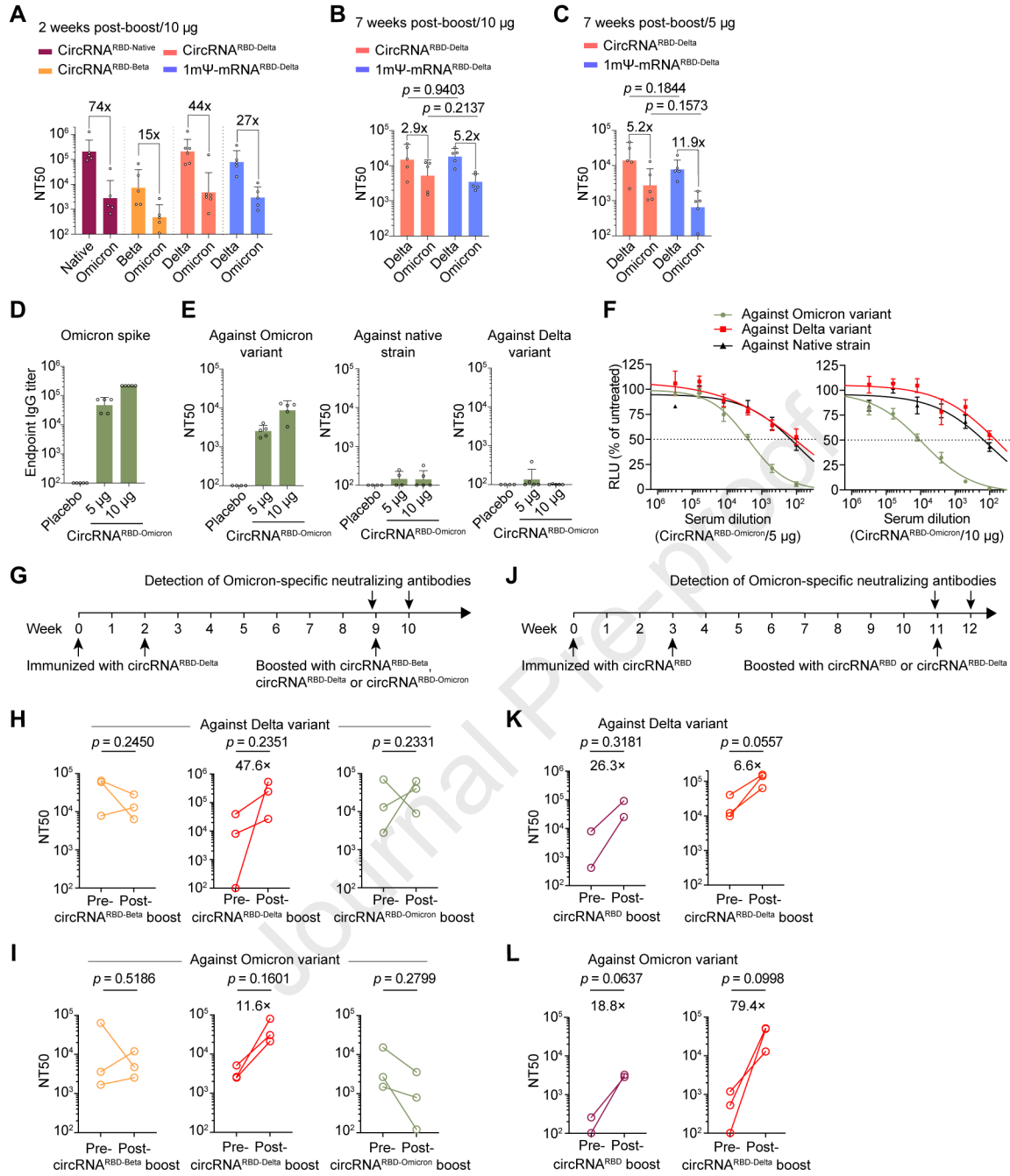
- 1387 Yang, J., Wang, W., Chen, Z., Lu, S., Yang, F., Bi, Z., Bao, L., Mo, F., Li, X., Huang, Y., *et al.* (2020). A vaccine
1388 targeting the RBD of the S protein of SARS-CoV-2 induces protective immunity. *Nature* 586, 572-577.
- 1389 Yang, Y., Fan, X., Mao, M., Song, X., Wu, P., Zhang, Y., Jin, Y., Yang, Y., Chen, L.L., Wang, Y., *et al.* (2017).
1390 Extensive translation of circular RNAs driven by N(6)-methyladenosine. *Cell Res* 27, 626-641.
- 1391 Yu, J., Tostanoski, L.H., Peter, L., Mercado, N.B., McMahan, K., Mahrokhian, S.H., Nkolola, J.P., Liu, J., Li, Z.,
1392 Chandrashekar, A., *et al.* (2020). DNA vaccine protection against SARS-CoV-2 in rhesus macaques. *Science* 369,
1393 806-811.
- 1394 Zhang, M., Huang, N., Yang, X., Luo, J., Yan, S., Xiao, F., Chen, W., Gao, X., Zhao, K., Zhou, H., *et al.* (2018a). A
1395 novel protein encoded by the circular form of the SHPRH gene suppresses glioma tumorigenesis. *Oncogene* 37,
1396 1805-1814.
- 1397 Zhang, M., Zhao, K., Xu, X., Yang, Y., Yan, S., Wei, P., Liu, H., Xu, J., Xiao, F., Zhou, H., *et al.* (2018b). A
1398 peptide encoded by circular form of LINC-PINT suppresses oncogenic transcriptional elongation in glioblastoma.
1399 *Nat Commun* 9, 4475.
- 1400 Zhang, N.N., Li, X.F., Deng, Y.Q., Zhao, H., Huang, Y.J., Yang, G., Huang, W.J., Gao, P., Zhou, C., Zhang, R.R.,
1401 *et al.* (2020). A Thermostable mRNA Vaccine against COVID-19. *Cell* 182, 1271-1283 e1216.
- 1402 Zhang, X.O., Wang, H.B., Zhang, Y., Lu, X., Chen, L.L., and Yang, L. (2014). Complementary sequence-mediated
1403 exon circularization. *Cell* 159, 134-147.
- 1404 Zhou, P., Yang, X.L., Wang, X.G., Hu, B., Zhang, L., Zhang, W., Si, H.R., Zhu, Y., Li, B., Huang, C.L., *et al.*
1405 (2020). A pneumonia outbreak associated with a new coronavirus of probable bat origin. *Nature* 579, 270-273.
- 1406 Zhu, F.C., Li, Y.H., Guan, X.H., Hou, L.H., Wang, W.J., Li, J.X., Wu, S.P., Wang, B.S., Wang, Z., Wang, L., *et al.*
1407 (2020). Safety, tolerability, and immunogenicity of a recombinant adenovirus type-5 vectored COVID-19 vaccine: a
1408 dose-escalation, open-label, non-randomised, first-in-human trial. *Lancet* 395, 1845-1854.
- 1409

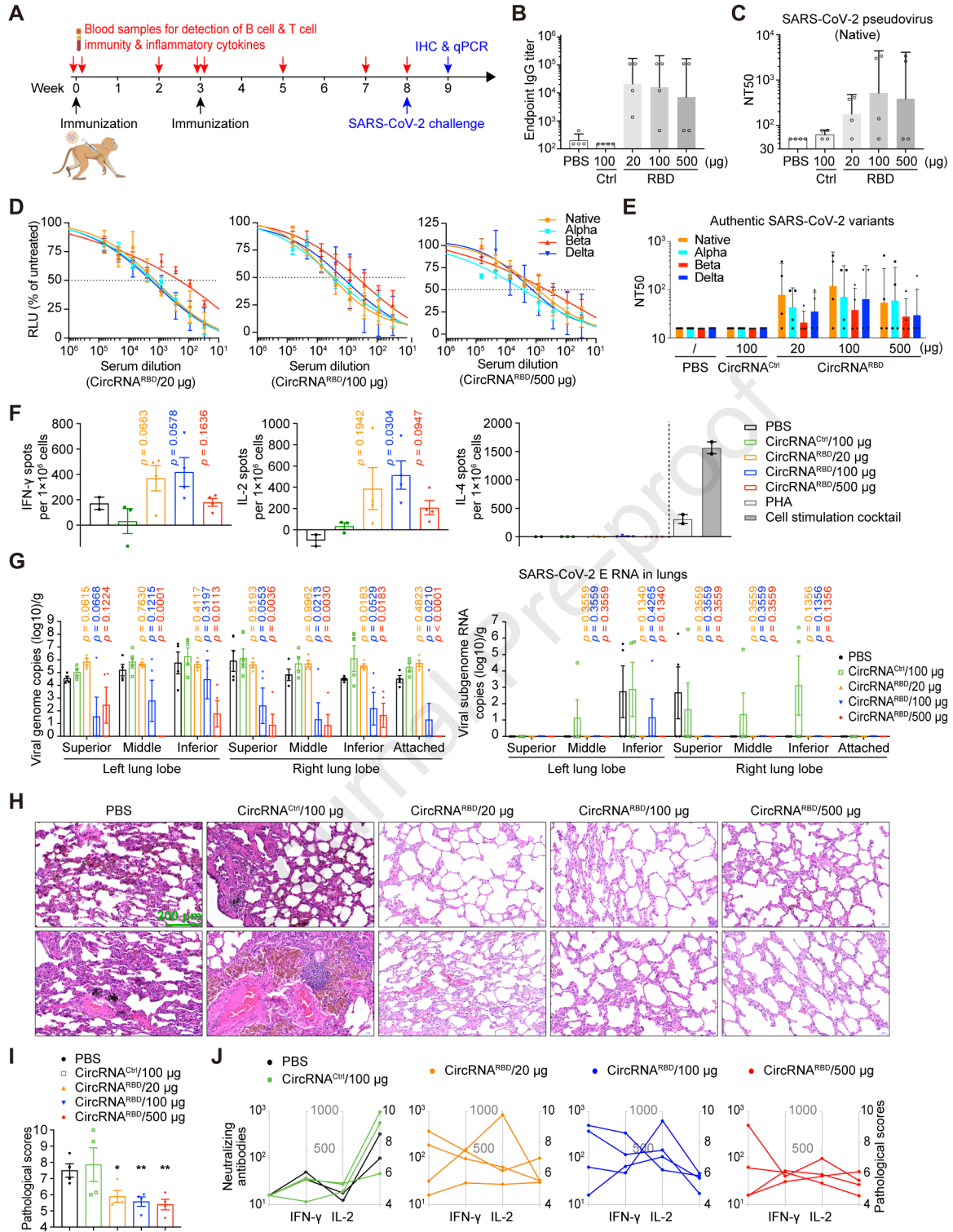


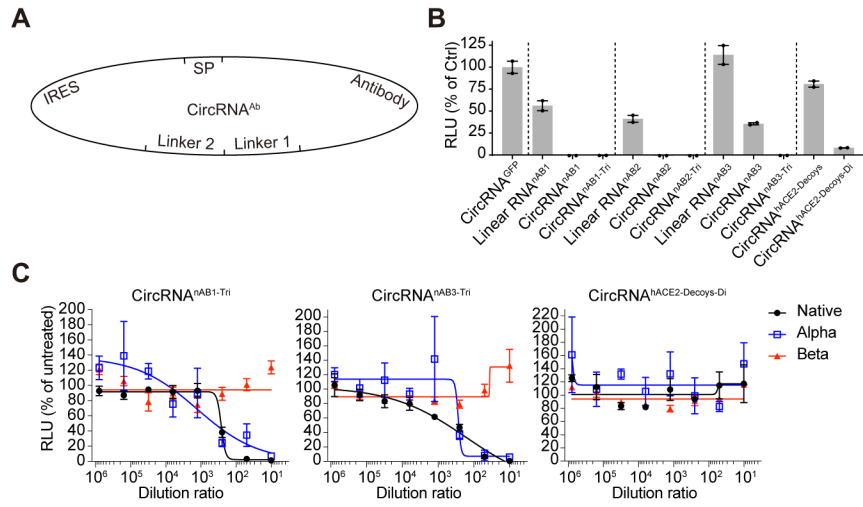












Circular RNA Vaccines against SARS-CoV-2 and Emerging Variants

Authors

Liang Qu, Zongyi Yi, Yong Shen, ..., Jianwei Wang, Xiaoliang Sunney Xie, Wensheng Wei

Correspondence

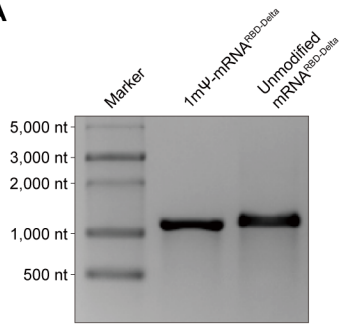
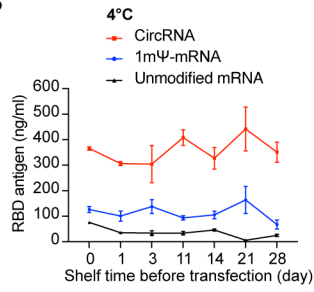
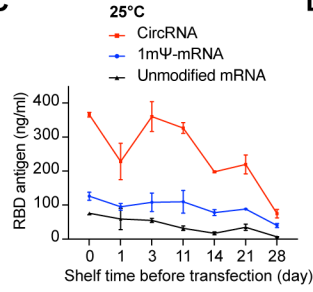
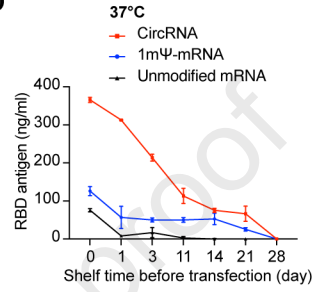
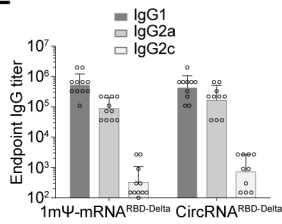
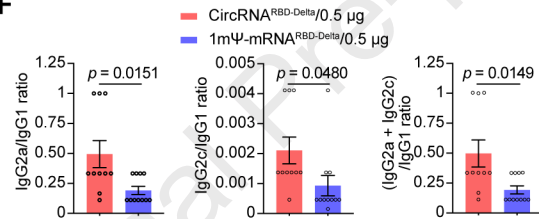
wswei@pku.edu.cn (W.W.)

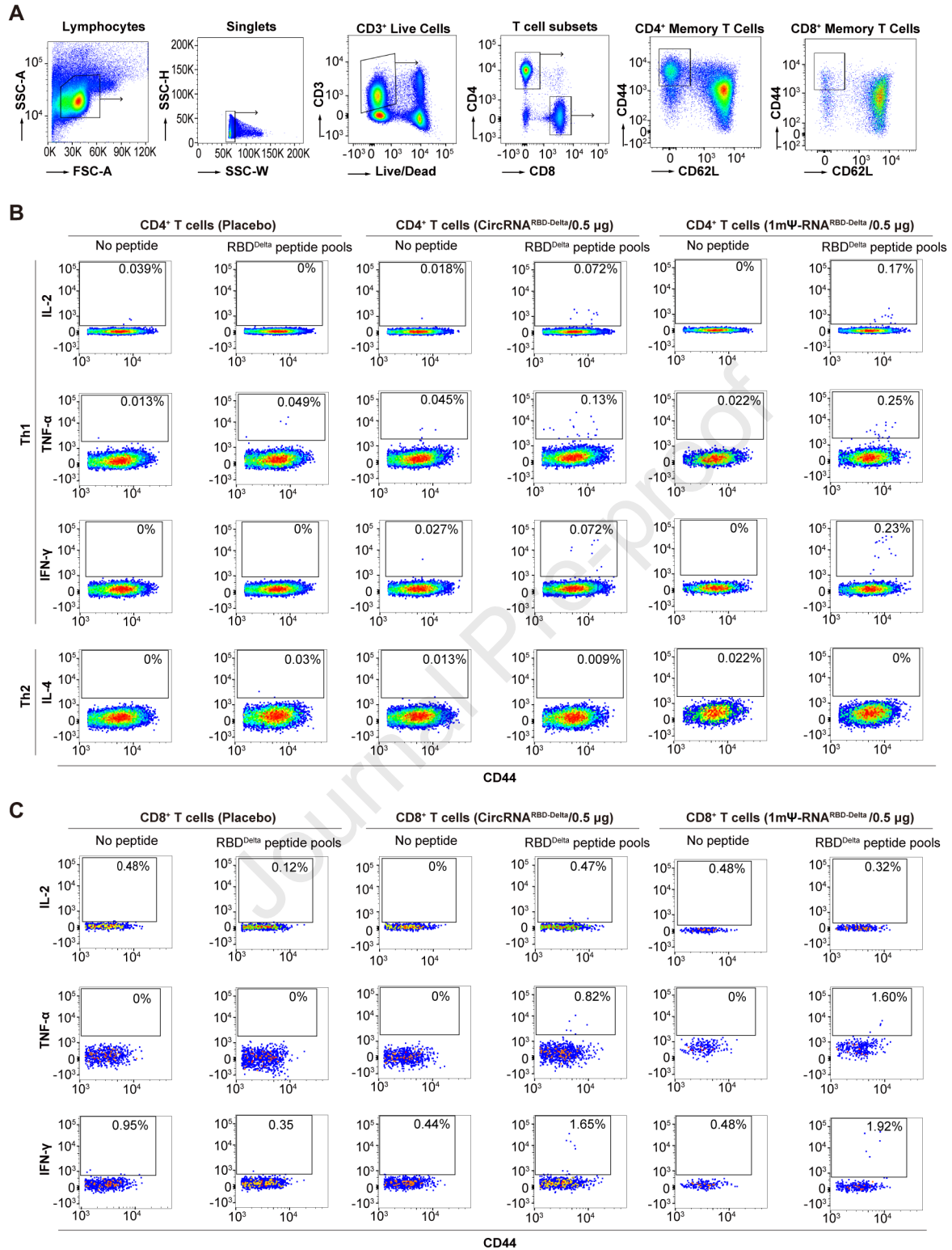
In Brief

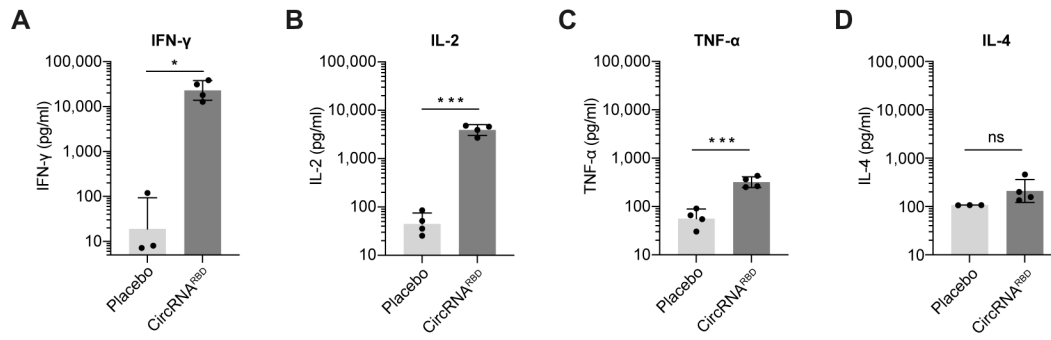
A circular RNA (circRNA) vaccine that encodes the trimeric RBD antigens of SARS-CoV-2 spike provides protection and memory boosting against SARS-CoV-2 variants of concern, in mice and rhesus macaques.

Highlights

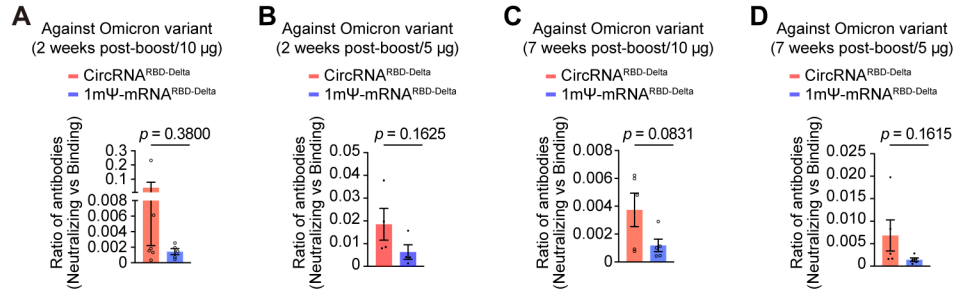
- Highly stable circRNA vaccines induce potent humoral and cellular immune responses
- CircRNA vaccines elicit a high proportion of neutralizing antibodies
- CircRNA vaccines enable effective protection against SARS-CoV-2 in mice and monkeys
- CircRNA^{RBD-Delta} vaccine provides broad-spectrum protection against SARS-CoV-2 VOCs

A**B****C****D****E****F**





Journal Pre-proof



Journal Pre-proof

